Atomization and Sprays, vol. 17, pp. 1–45, 2007

UNSTEADY RANS MODELING OF WATER-SPRAY SUPPRESSION FOR LARGE-SCALE COMPARTMENT POOL FIRES

Sam S. Yoon* and Ho Young Kim
Mechanical Engineering Department, Korea University, Anamdong, Seoul, Korea

Paul E. DesJardin
Department of Mechanical and Aerospace Engineering, University at Buffalo, the State University of New York, New York, NY

John C. Hewson, Sheldon R. Tieszen, and Thomas K Blanchat
Fire Science & Technologies, Sandia National Laboratories, Albuquerque, NM

Original Manuscript Submitted: 7/28/2005; Final Draft Received: 11/12/2005

This paper presents a computational study of the effect of water-spray characteristics on the suppression of a large-scale (2 m × 2 m) JP-8 pool fire in a 10 m × 10 m × 10 m compartment with an open ceiling. The numerical model is based on an unsteady Reynolds-averaged Navier–Stokes formulation using a stochastic separated flow approach for the droplets that includes detailed descriptions of the interaction between water droplets and fire plume. Simulation results indicate that water-spray injection causes the gas temperature to rise due to the initial enhancement of the turbulent mixing. A threshold suppression condition is achieved when the injected droplet carries enough momentum (injection speed range is 20–80 m/s) to penetrate the fire plume and evaporate in the flame regions where most of the gas-phase combustion is taking place. In addition, the droplet size (ranging from 100–800 μm) should be small enough to yield quick evaporation when in contact with the flame surface for efficient cooling. Based on a parametric study, a preferred fire suppression configuration is recommended for the systems considered.

*Corresponding author; e-mail: skyoon@korea.ac.kr

INTRODUCTION

Uncontrolled fires have devastated both human life and property throughout history. While water has always been seen as a possible suppression method, interest in the use of water for fire suppression has recently been renewed by the signing of the Montreal Protocol in 1987, prohibiting the use of the popular suppressants Halon 1301 (CF_3Br) and 1202 (CF_2Br_2) because they were found to deplete the ozone layer. The use of water sprays continues to be a leading candidate for Halon replacement because it is environmentally friendly, nontoxic, and inexpensive.

Because of water's high efficiency in extracting energy during its phase transformation from liquid to vapor, high local gas fire temperatures can be substantially reduced. This temperature reduction reduces fuel devolatilization or evaporation, and suppression occurs. In addition, the vaporized water occupies the local space, displacing the local oxygen concentration and preventing reignition [1].

The objective of this study is to consider the use of a high-speed water spray, which substantially reduces the heat flux radiated to the fuel surface by distorting the fire geometry [2]; the shape of the combustion zone can be distorted using a water-spray momentum greater than the momentum of the fire buoyancy force. It is crucial to provide the droplet size capable of delivering sufficient momentum to overcome the fire buoyancy force. For this reason, we have conducted a series of simulations in which we vary the mean droplet size of the water-spray system, as well as the spray injection speed. Here, we define that the optimum fire suppression condition is found when the selected local flame temperature is reduced to a room temperature of 300 K at the fastest rate with respect to other cases under the fixed amount of water supply (i.e., fixed water mass flow rate).

The scope of this study is limited to understanding the key physics parameters in gas-phase fire suppression from sprinklers (or water mist systems), which are commonly deployed in a ceiling mounted configuration. This study uses commonly used engineering subgrid scale (SGS) models [3], rather than seeking the advancement of new SGS models [4].

The models will be discussed following a selected literature review in the next section. The model performance against a selected data set will then be demonstrated. A parametric study showing the effects of spray jet momentum and droplet size will be given. Finally, conclusions are drawn on initial spray momentum, droplet sizes, and nozzle configuration that result in preferred fire suppression.

LITERATURE REIVEW

Fire associated with large-scale liquid fuel dispersion has received much attention recently because its prevention is of interest to civilian, military, and government agencies for safety and reliability issues in a wide range of practical applications such as moving vehicle collisions with flammable storage (i.e., gas station, liquid natural gas facilities, gas/oil pipeline) or a moving fuel tank crashing against a building (i.e., the 9/11 terrorist attack). It is crucial to understand the physics of fuel-vapor formation, its ignition, and subsequent burning as a function of scale because a different fire suppression system is needed, depending on the given physical scale of the fire; allowing highly reliable fire suppression systems to be designed.

A nonpremixed diffusion fire (such as a hydrocarbon pool fire) is generally buoyancy driven flow. The density of the hot flame zone is lower than that of the surrounding atmosphere, which causes the vortice roll-up motion at the fire-air interface, as shown in Fig. 1a. This periodic roll-up motion is called "puffing." The subsequent 3D "finger" formation [4] also occurs, whose phenomenon is known as the Rayleigh–Taylor instability, as shown in Fig. 1b.

It is worthwhile to present a general overview of fire suppression studies as a useful guidance for readers. The suppression of a hydrocarbon pool fire is generally of great interest to the fire suppression community. A review of both modeling and experimental studies that focus on transport and suppression processes associated with gas-phase fire suppression by water mist systems is provided in this section. Summaries of these studies grouped into suppression of laminar flames, gaseous plume fires, pool fires, and compartment fires are given in Tables 1–3.

Small-Scale Flame Suppression

Due to the large length scale range between flame sheets and buildings, studies are often done at two scales, namely, laminar or flame-scale studies, and turbulent or large-scale studies. This section reviews selected small-scale gas-phase suppression flame-scale studies.

Lentati and Chelliah [5] developed a two-phase Eulerian–Lagrangian fire suppression model based on the axisymmetric laminar gas-phase Navier–Stokes solver. The counterflow (or impinging flow) between the water spray and the methane plume was studied by Lentati and Chelliah [5]. They showed that small droplets (i.e., <20 μm) went through quick evaporation in the mixing layer and never crossed the stagnation plane. A droplet size of at least 50 μm or greater was needed to penetrate into the flame while over-

a)

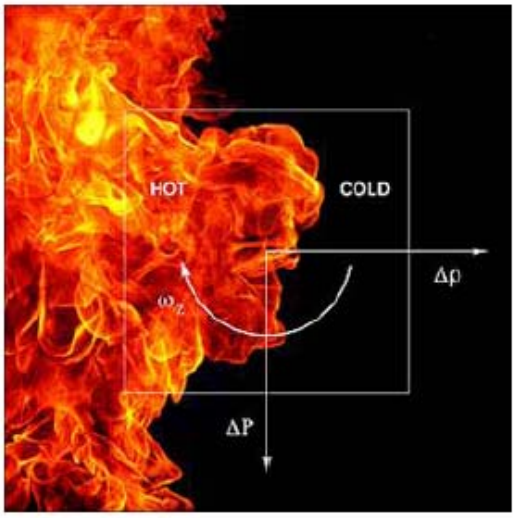

b)

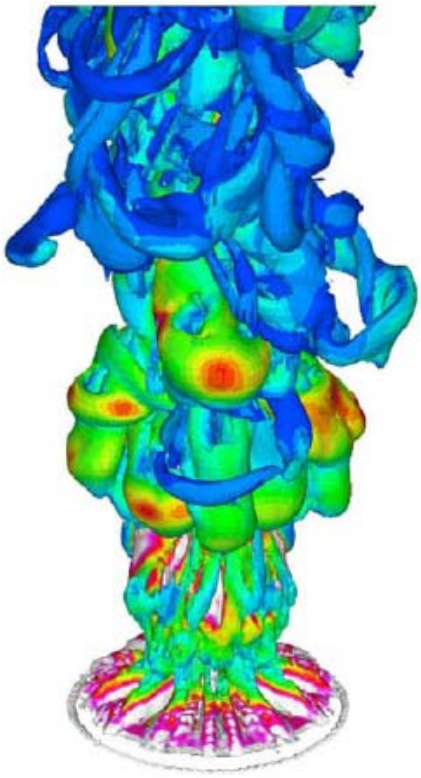

Fig. 1 (a) Baroclinic torque of the buoyancy driven instability of a fire flame. (b) Instantaneous snapshot of puff cycle from LES showing isosurfaces of vorticity [4]. Printed with the permission of *American Institute of Physics*.

Table 1 History of Methane Gas Fire Suppression Experiment and Modeling Using Water–Mist Spray Systems. Note that D_{32} is the Sauter Mean Diameter

Source	Experiment/ modeling	Comments
McCaffrey [14]	Experiment	7 MW methane diffusion flame. Base spray injection
Downie and Polymeropoulos [15]	Experiment	0.25 m × 0.25 m square methane burner area. 250 μm < D_{32} < 270 μm, $\dot{m} = 0.013$ kg/s
Lentati and Chelliah [5]	Modeling	Steady, laminar counterflow methane-air diffusion flame. D < 100 μm
Ndubizu et al. [48]	Experiment	2D coaxial methane–air diffusion flame. 28 μm < D_{32} < 66 μm, ΔP = 483 kPa
Prasad et al. [7, 8]	Modeling	2D coaxial methane–air diffusion flame. D = 50, 150 μm (monospray), 0.25 m/s < U_{inj} < 50 m/s
Lazzarini et al. [9]	Experiment	Experiment Methane diffusion flame. $D_{32} \sim 30$ μm
Chelliah et al. [10]	Experiment	Methane diffusion flame. $D_{32} \sim 30$ μm
Thomas [11]	Modeling	Methane diffusion flame. D = 10, 20, 30, 50, 100 μm (mono-spray).
Heskestad [16]	Experiment	Methane diffusion flame. 165 μm < D_{32} < 330 μm

Table 2 History of Liquid Pool Fire Suppression Experiments and Modeling Using Water–Mist Spray Systems

Source	Experiment/ modeling	Comments
Rasbash and Rogowski [18]	Experiment	0.3 m diameter kerosene pool fire. ΔP < 690 kPa, 300 μm < D < 3000 μm
Rasbash et al. [2]	Experiment	0.3 m diameter kerosene pool fire. ΔP < 690 kPa, 300 μm < D < 3000 μm
Prasad et al. [12]	Modeling	1 cm unit length (2D) methanol pool fire. D = 50, 150 μm (monospray)
Jianghong et al. [19]	Experiment	5 cm diameter ethanol and kerosene pool fire. D_{32} = 80 μm, 0.0008 kg/s < $\dot{m}$ < 0.0016 kg/s

Table 3 History of Compartment Fire Suppression Modeling Using Water–Mist Spray Systems

Source	Liquid-phase model	Gas-phase model
Alpert [20]	Lagrangian poly disperse spray	k–ε turbulent, 2D using 20 × 20 nodes for 15 m × 10 m domain
Hoffman and Galea [21, 22]	Eulerian monodisperse spray	k–ε turbulent, 3D using 12 × 11 × 20 nodes for 2.44 m × 3.66 m × 2.44 m domain
Chow and Fong [24]	Lagrangian polydisperse spray	k–ε turbulent, 3D using 51 × 9 × 19 nodes for 27 m × 3 m × 6 m domain
Novozhilov et al. [29]	Lagrangian monodisperse spray	k–ε turbulent, 3D using 30 × 27 × 20 nodes for 6.0 m × 5.4 m × 2.4 m domain
Nam [27]	Lagrangian monodisperse spray	k–ε turbulent, 2D using 60 × 60 nodes for 7.88 m × 3.86 m domain
DesJardin et al. [30]	Lagrangian polydisperse spray	k–ε turbulent, 3D using 34 × 30 × 37 nodes for 3.05 m × 3.05 m × 3.05 m domain
Chow and Yao [35]	Axisymmetric polydisperse spray	1D control volume analysis
Hua et al. [37]	Lagrangian monodisperse spray	k–ε turbulent, 2D using 30 × 30 nodes for 2 m × 2 m domain
Prasad et al. [38]	Eulerian monodisperse	k–ε turbulent, 3D using 36 × 24 × 24 nodes for 3.7 m × 2.5 m × 2.5 m domain
Vaari [39]	Axisymmetric polydisperse spray	1D control volume analysis
Consalvi et al. [40]	Eulerian monodisperse spray	k–ε turbulent, 2D using 90 × 50 nodes for 7 m × 3 m domain
Kim and Ryou [42]	Lagrangian polydisperse spray	LES turbulent, 3D using 84 × 84 × 48 nodes for 4.0 m × 4.0 m × 2.3 m domain
Li and Chow [44]	Axisymmetric polydisperse spray	1D control volume analysis

coming the buoyancy force of the fire plume for the given spray operating condition and fire size.

The Ndubizu et al. [6] experimental study was on the parallel coaxial flow between water spray and a 2D methane diffusion flame. The study indicated that in a coaxial-flow arrangement, water spray had more of a gas-phase cooling effect than an oxygen dilution effect on the flame.

Prasad et al. [7] also studied the coaxial-flow fire suppression case. Their numerical study was based on the 2D Eulerian-Eulerian approach, where the droplet diameter, throw angle, particle number density, and spray injection velocity were varied to yield an optimum fire suppression condition. They also found that the suppression efficiency increased with higher particle number density or with higher water-spray injection velocity. The supplementary work in Prasad et al. [8] gives more detailed information.

Lazzarini et al. [9] conducted an experimental study on the case considered in Lentati and Chelliah [5] to validate their numerical code. The results of the model and the experimental data agreed well. The experimental study also showed that suppression could be better optimized using water suppressant mixed with the compound NaOH, which complements the thermal effects with the chemical catalytic radical recombination effects of NaOH. Additional experimental studies are found in Chelliah et al. [10]. A similar methane flame suppression numerical study is found in Thomas [11].

Prasad et al. [12] performed a 2D numerical modeling on a laminar methanol pool fire (1 cm in width) and its suppression using water spray. They also found that the smaller droplet size extinguished the fire more efficiently when the water spray was injected from beneath the pool fire (base injection) because the small droplets were entrained into the fuel surface more readily due to their smaller relaxation time with respect to the gas phase [13]. Suppression was achieved by the mechanism of thermal cooling (i.e., absorbing heat from the fire to the water droplets by means of droplet evaporation) and the subsequent oxygen displacement effect when water vapor was produced. The coaxial air flow was intentionally injected with water spray to stabilize the pulsating pool fire, which pushed the vortical structures further away from the burner surface.

Gaseous-Plume Fire Suppression

A suppression study of a relatively large-scale methane-vapor fire (7 MW) was conducted by McCaffrey [14]. Flame heights, centerline temperatures, and incident radiative flux were measured with and without water-spray suppressant. McCaffrey's experimental study indicated that the local

flame temperature could increase during the water-spray injection below the flame exit because of the increased emissivity of the radiatively active water steam and the abundant oxygen supply due to the air entrainment during the spray injection below the flame exit.

Downie and Polymeropoulos [15] also studied the water-spray suppression of a methane diffusion flame. Their study showed that suppression was achieved, not by reducing the flame temperature itself, but rather by reducing the oxygen concentration at the burner surface by replacing the oxygen volume with the evaporated water steam.

Heskestad [16] provided a correlation for an optimized nozzle diameter in terms of water-spray mass flow rate and discharging water momentum. A reasonably good comparison was observed between the correlation and the experiment conducted using a methane gas plume of 0.1–0.3 m diameter.

Pool Fire Suppression

Pool fire suppression has probably received more attention than gaseous fire suppression due to its practical applications, which can be observed in any fuel-spill accident scenario. Generally, a pool fire produces more smoke than a fire with a gaseous fuel because of the higher sooting propensity of most liquid fuels and the long mixing time scales associated with buoyancy-driven vortex roll up [17].

Early pool fire suppression work can be found in Rasbash and Rogowski [18]. Their kerosene pool fire (30 cm in diameter) was cooled by water sprays projected downward. Rasbash and Rogowski [18] suspected that the core cooling mechanism was the abstraction of heat from the fuel by water droplets within the fuel. The authors also found that the ability of the water spray to remove heat increased as the flow rate of the water spray increased. Their following study in Rashbash et al. [2] found that a spray system that produced a smaller droplet size was more efficient in extinguishing the same kerosene pool fire of 30 cm in diameter when the spray was injected at an angle of 60 deg at a lower height. Their previous study had used a 90 deg angle, the spray nozzle projecting downward to the pool fire flame. The latter study indicated that the variation of water droplets' evaporation rate (depending on their size) was an important parameter in order to achieve an efficient fire suppression condition.

Jianghong et al. [19] experimentally investigated a 5 cm diameter ethanol and kerosene pool fire. A water spray was located 30 cm above the pool fire and initiated 100 s after ignition. It was found that more rapid suppres-

sion was achieved when the mass flow rate of the water spray increased. It also was noted that the fire intensified due to the enhanced mixing of the fuel and air when the water-spray mass flow rate was smaller, and suppression was not achieved.

Compartment Fire Suppression (Modeling)

Modeling is useful for providing insight into large fire experiments, which may be expensive and dangerous to conduct. Over the past two decades, the computational aspect of large-scale fire suppression has received much attention not only because of the high cost associated with actual experiments, but also because the research itself-fire suppression is a relatively new area for the computational research community [1]. Generally, fire suppression in a compartment is of great interest to the community because of its practical applications, such as in structure and vehicle fires. Table 3 summarizes these studies.

Alpert [20] presented 2D numerical results on the suppression of a methane gas compartment fire. It was found that the heat absorbed by the water spray increased when the spray mass flow rate increased, a pattern consistent with the experimental observation of Jianghong et al. [19].

Hoffmann and Galea [21, 22] developed 3D modeling for a compartment fire suppression application. In their study, the wastepaper basket fire scenario was assumed with a power output up to 50 kW. The local gas temperature history of the numerical simulation was compared with the experimental data of Cooper and Stroup [23].

Chow and Fong [24] presented a more complete and detailed modeling description for the 3D modeling of compartment fire suppression. The Lagrangian approach of Dukowicz [25] was adopted for the liquid phase and the k–ε turbulence RANS model was used for the gas phase. The mass, momentum, and heat transfer effects were taken into account through the particle source in cell (PSI-CELL) algorithm of Thomas [11] and Crowe et al. [26].

Nam [27] investigated the penetration capability of water spray by varying the mass flow rate using the axisymmetric code, which also utilized Crowe's PSI-CELL algorithm [26] and the SIMPLE algorithm [28]. The study indicated that fire suppression was very sensitive to the spray initial conditions such as the droplet size and velocity.

Novozhilov et al. [29] also used the PSI-CELL algorithm for modeling coupling effects between the liquid and the gas phase. The Lagrangian droplet tracking approach was used for the liquid phase and the SIMPLE algorithm for the gas phase. The burning rate and extinguishment of PMMA

(polymethylmethacrylate) in a compartment were obtained and compared with the experimental data.

DesJardin et al. [30] also used the PSI-CELL and SIMPLE algorithms for their 3D pool fire suppression simulation. The fuel was heptane located on a square burner, 0.3 m × 0.3 m. The droplet evaporation was modeled using the Ranz–Marshall correlations [31, 32], which utilized Clausius-Clapeyron [33] and Watson's [34] relation for approximating the droplet film properties. The numerical results from DesJardin et al. [30] indicated that turbulent mixing of the flame was enhanced (thus, the local temperature increased temporarily) on spray injection.

Chow and Yao [35] presented a computationally efficient and simple two-layer model for the fire suppression case. The dynamics of water droplets for the noncombustion and nonsuppression case was validated against the experimental data of St-Georges and Buchlin [36]. Then the two-layer model was extended to the suppression case where the local gas temperature was predicted at various downstream locations.

Hua et al. [37] performed parametric studies to optimize the fire suppression of a methane gas plume from a square burner, 0.25 m × 0.25 m. The initial droplet size, the spray pattern (i.e., solid cone, hollow spray), and the mass flow rate were varied. It was found that the water spray with a solid cone pattern and finer water droplet size was more effective in extinguishing fires than the one with a hollow cone pattern and coarse water droplet size.

Prasad et al. [38] also performed parametric studies to optimize the various water-spray injection characteristics such as droplet diameter, injection density injection velocity, and nozzle orientation on mist entrainment and suppression. Numerical studies indicated that for similar values of injection parameters, the time for suppression was smallest for the top injection configuration for the large-scale (0.61 m × 1.22 m square burner) turbulent propane pool fire, contradicting the previously reported data in Prasad et al. [12]. In the previous paper [12], the bottom (or base) injection was shown to better suppress small-scale (1 cm in length) laminar methanol pool fires. This difference indicated that the nature of small-scale fire suppression is intrinsically different from that of large-scale fire suppression.

Vaari [39] proposed a transient one-zone computer model for total flooding water mist fire suppression in ventilated enclosures. The model solved the time evolution of temperature, gas density, gas composition, and water mist concentration inside the protected space. The extinguishment of a hydrocarbon pool fire was predicted based on the adiabatic flame temperature concept.

Consalvi et al. [40] used a newer version of the k–ε model, the RNG k–ε model developed by Yakhot and Orszag [41], to model both gas and liquid phases using a two-continuum phase assumption, an Eulerian-Eulerian model. The study demonstrated the 2D simulation capability on the suppression of a 0.2 m length ethylene diffusion flame, which produced 100 kW power output. It also revealed that thermal cooling (i.e., absorbing heat from fire to water droplet by the means of droplet evaporation) was the main driving mechanism for suppression. It was also found that the radiation energy emitted by the flame was reduced, and the energy was attenuated, by water droplets. Temporary fire enhancement due to intensified turbulence mixing was observed when the spray injection was initiated, as previously reported by DesJardin et al. [30] and Jianghong et al. [19].

Kim and Ryou [42] used the LES model of McGrattan et al. [43] for their suppression study for a hexane pool fire of 0.3 m × 0.3 m in a compartment. Direct cooling of the fuel surface was found to be the driving mechanism for suppression when the spray momentum was large enough to overcome the buoyancy force of the plume. Oxygen displacement due to water vapor formation was the driving suppression mechanism when the spray momentum was not sufficient to push the stagnation region near to a floor.

Li and Chow [44] proposed a 1D suppression model, similar to that of Chow and Yao [35] and Vaari [39]. Li and Chow's model was developed for fire scenarios where oxygen depletion was the dominant mechanism of fire extinguishment and was implemented with a more robust drag model, as compared to the previous models of Chow and Yao [35] and Vaari [39].

Compartment Fire Suppression (Experiment)

Available literature on compartment fire suppression experiments are listed in Table 4. Kung [45] conducted an experiment of a 0.914 m diameter hexane pool fire in a compartment. The study indicated that the rate of water droplet evaporation was directly proportional to the heat release rate and the mass flow rate, so that the spray mass flow rate, droplet size of the spray, and heat release rate of the fire source were the controlling parameters in the cooling of a compartment fire.

The experimental study of Cooper and Stroup [23] dealt with a paper waste fire in a compartment size of 3.66 m × 2.44 m × 2.44 m, producing a maximum heat release rate of 65 kW. Consalvi et al. [40] used this particular experimental data set for model validation work because of its useful measurements of the local gas temperature and heat flux. The experimental work focused attention on key features of the typical sprinkler link deploy-

Table 4 History of Compartment Fire Suppression Experiments Using Water–Mist Spray System

Source	Fire size	Fuel	Spray mass flowrate	Injection period	Injection speed Initial drop size	Comments
Kung [45]	Pan diameter = 0.762, 0.914 m	Hexane	$0.448 < \dot{m} < 1.08$ kg/s	$\Delta t < 60$ s	$5 \le U_{inj} \le 32$ m/s $4 < D_{32} < 11$ mm	3.05 m × 3.66 m × 2.45 m with 1.5 m × 1.1 m open window
Cooper and Stroup [23]	65 kW	Paper	$\dot{m} = 0.596$ kg/s	$\Delta t < 25$ s	$U_{inj} = 10$ m/s D_{32} unknown	Confined room (3.66 m × 2.44 m × 2.44 m) with an open door (0.76 m × 2.03 m)
Kim et al. [46]	Pan diameter = 0.1 m	Gasoline	$\dot{m} \le 0.0105$ kg/s	$\Delta t = 0.43$ s	$U_{inj} = 37$ m/s $D_{32} < 70$ μm	Small laminar flame
Back et al. [47]	$0.25 \le$ Pan area ≤ 0.41 m^2	Heptane	$0.4 \le \dot{m} \le 1.3$ kg/s	$\Delta t =$ 84–436 s	$49 \le U_{inj} \le 141$ m/s $D_{32} < 100$ μm	5 m × 7 m × 3 m machinery space with 1.7 m^2 open vent at 25 m^3/min air flow rate
Ndubizu et al. [48]	Pan diameter = 0.5 m	Heptane Hydrocarbon	$0.1 \le \dot{m} \le 0.7$k g/s	$\Delta t =$ 300 s	$13 \le U_{inj} \le 41$ m/s $58 < D_{32} < 215$ μm	7.6 m × 7.0 m × 8.0 m building with open ceiling
Marker and Reinhardt [49]	16 large and 8 small boxes, filled with shredded paper	Paper	$0.025 \le \dot{m} \le 0.0417$ kg/s	$\Delta t =$ 5340 s	$23 < U_{inj} < 29$ m/s $D_{32} = 100$ μm	57 m^3 air cargo compartment, used twin-fluids effervescent spray
Chow et al. [50]	Pan diameter = 0.2, 0.35, 0.5 m	Gasoline	$0.020 \le \dot{m} \le 0.022$ kg/s	$\Delta t =$ 110–508 s	$U_{inj} \sim 58$ m/s $D_{32} = 340$ μm	Confined room (3.6 m × 2.4 m × 2.4 m) with an open door (0.8 m × 1.95 m)

ment and response problem. The study revealed that the elevated temperature of upper smoke layers that developed in compartment fires could have a major impact on the thermal response of sprinkler links.

Kim et al. [46] conducted an experiment on a relatively small gasoline pool fire (0.1 m diameter) in a compartment. The fire was rapidly extinguished by the relatively high-speed injector (U_{inj} = 37 m/s) in a period of less than 1 s. The fire extinction limit was obtained as a function of the measured injector pressure when the fire was extinguished. The burning rate of the fuel was also measured. This experimental study indicated that effective water flux was more useful than injection pressure in fire extinguishment. It was also revealed that a larger spray thrust induced a faster burning rate due to a greater supply of air through entrainment.

Back et al. [47] evaluated the fire suppression system used to protect small (~100 m^3) machinery space applications. The primary objective of the investigation was to evaluate the applicability of the International Maritime Organization's (IMO) test protocol and design requirements for smaller machinery spaces, and for machinery spaces with combustible boundaries. The study showed that combustible boundaries did not pose a significant challenge to water mist systems. It was also found that oxygen depletion due to water vapor formation, which caused a rapid reduction in the burning rate of the fire, was the main driving mechanism for suppression.

Ndubizu et al. [48] presented experimental parametric suppression studies of 0.5 m diameter heptane and hydrocarbon pool fires in a compartment. The study showed that base injection of water droplets yielded more effective suppression conditions than top injection, consistent with the observation of the Prasad et al. [12] for the relatively small-scale < 1 cm width) methanol pool fire simulation. However, the latter work of Prasad et al. [38] showed that top injection was a better arrangement for a suppression system for large-scale (0.61 m × 1.22 m square burner) turbulent propane pool fires. Ndubizu et al. [48] noted that oxygen depletion and direct fuel surface cooling were the main driving suppression mechanisms.

Marker and Reinhardt [49] reported full-scale fire tests to investigate the effectiveness of several types of water-spray systems against in-flight cargo compartment fires. Several spray injector types were evaluated. It was found that direct thermal cooling from heat absorption of evaporating water droplets was the main suppression mechanism. The cargo size was 57 m^3 and paper waste was used as a combustion source. The suppression time (or fire duration) was long relative to other compartment suppression studies described here due to the low mass flow rate of the water spray applied.

Chow et al. [50] conducted a gasoline pool compartment fire experiment whose heat release rate reached 300 kW. Chow et al. [50] noted that the shape and geometry of a fire controlled the heat flux radiated to the fuel surface and, thus, the amount of vapor formation was also affected by the fire shape. For this reason, the distortion in fire shape due to water spray can contribute to rapid suppression. In essence, pushing the flame sideways with a discharged water mist reduces the normal thermal feedback to the pool and therefore results in the extinguishment. Chow et al. [50] also noted that the effect of the ratio between the pool diameter and depth was important to understand since suppression was more difficult to achieve for a low diameter/depth ratio.

MODELING DESCRIPTIONS

Numerical simulations are conducted using Sandia's fire field modeling code, VULCAN. The Eulerian gas-phase system is based on an unsteady Reynolds-averaged Navier–Stokes (RANS) formulation employing a standard k–ε isotropic turbulence closure model [51]. The "eddy dissipation concept" (EDC) combustion model of Ertesvag and Magnussen [52] is used to model turbulent combustion as extended by Tieszen and Black [53] and Hewson et al. [54] to include the effects of flame suppression. Details of the flame suppression will be given in the next section. Soot formulation and absorption properties are based on the work of Tesner [55], and a discrete transfer method is used to solve for the radiation heat transfer.

The gas-phase flow is calculated on a Eulerian staggered Cartesian grid using the pressure correction method of the SIMPLE algorithm [28]. The second-order upwinding and centered schemes are used for the convective and diffusion terms, respectively, in solving the transport differential equations.

The water-spray model is based on a Lagrangian stochastic separated flow approach [56, 57]. Evolution equations for collections of droplets with similar sizes and initial conditions, denoted as parcels, are used to reduce computational cost. The parcels are advanced under the influence of modeled turbulent fluctuations in the gas-phase properties. Maxey and Riley's [58] momentum equation for a small rigid sphere in a nonuniform flow is used, as well as the drag model of Chhabra et al. [59] and the correlation by Ganser [60]. Evaporation is modeled using a thin-skin model with standard convective correlations for heat and mass transfer. Droplet-droplet collisions are modeled using the model of Ko et al. [61]. This approach only accounts for either droplet-droplet "bouncing" or "coalescence," and not a droplet-droplet

"shattering" effect that produces additional drops. The shattering effect may become important for the head-to-head colliding sprays [62]. Since all droplets are moving in the same direction in our spray, shattering is highly unlikely to occur. Droplet breakup due to aerodynamic forces is modeled using the Taylor analogy breakup (TAB) model of O'Rourke and Amsden [63].

Turbulence models are introduced at the parcel and subparcel level to account for the effect of local fluctuations in the velocity field while the rest of the thermophysical variables are approximated by their corresponding time-averaged values. The velocity-fluctuation models serve to increase the droplet dispersion, mimicking the effects of unresolved turbulent eddies. These unresolved turbulent motions are significant for the present high-pressure spray that generates substantial turbulent kinetic energy. These unresolved turbulent motions are decomposed into parcel and subparcel models. The parcel turbulence model accounts for the effects of turbulent eddies perturbing the parcel trajectory and is based on the random walk model of Gosman and Ioannides [64], as modified by Shuen et al. [65]. Within a parcel, the spatial distribution of particles is assumed to be of Gaussian form. The standard deviation of this spatial distribution evolves with time for each parcel, as discussed by Zhou and Yao [66].

Lagrangian Liquid Droplet Spray Model

The droplet phase evolves using a Lagrangian approach based on the stochastic separated flow model [56, 57]. Evolution equations for collections of droplets with similar sizes and initial conditions, denoted as parcels, are used to reduce computational cost. The parcels are advanced under the influence of modeled turbulent fluctuations in the gas-phase properties. Maxey and Riley's [58] momentum equation for a small rigid sphere in a nonuniform flow is used, as well as the drag model of Chhabra et al. [59] and the correlation by Ganser [60]. Evaporation is modeled using a thin-skin model with standard convective correlations for heat and mass transfer. Further details may be found in DesJardin and Gritzo [56].

Conservation of Mass. The correlation by Ranz and Marshall [31, 32] is used for the evaporation model as follows:

$$\frac{dm_d}{dt} = \pi D \frac{\mu_f}{Sc_f}\left[2 + \frac{2}{3}\mathrm{Re}^{1/2}\, Sc_f^{1/3}\right]\ln\left(1 + B_m\right) \tag{1}$$

where m_d is the droplet mass, D is the droplet diameter, $Sc_f = \nu_f / D_M$ is the film Schmidt number, D_M is the mass diffusivity, $\mathrm{Re} = \rho_g d \left| \vec{u}_d - \vec{u}_g \right| / \mu_g$ is the droplet Reynolds number, and $B_m = (Y_f - Y_g)/(1 - Y_f)$ is the Spaulding or

mass transfer number that characterizes the concentration gradients at the film interface. In these and all subsequent expressions, the subscript g represents gas properties, d represents droplet properties, and f represents droplet film properties for the thin-film approximation of the liquid-gas interface at the droplet surface.

Conservation of Momentum. The momentum equation for a small rigid sphere in a nonuniform flow is derived by Maxey and Riley [58]. As discussed by Faeth [67], if the ratio of droplet to gas densities is large (i.e., $(\rho_d/\rho_g >> 1.0)$, then the predominant forces generally consist of the drag and body forces, leading to a relatively simple form of the momentum equation,

$$m\frac{d\vec{u}_d}{dt} = \frac{\pi}{8}\rho_g D^2 C_D \left|\vec{u}_g - \vec{u}_d\right| (\vec{u}_g - \vec{u}_d) + mg \tag{2}$$

where $\vec{u}_d$ is the droplet velocity and $\vec{u}_g$ is the gas-phase velocity around that particle, and ρ_g is the gas-phase density. The last term on the right is the body force term due to gravity. The coefficient of drag, C_D, is modeled using the standard drag coefficient relations for a sphere in a uniform flow [58, 67].

Conservation of Energy. The droplet temperature evolution is a balance between convection and evaporation. The droplet thermal energy can then be expressed as

$$mc_{v,d}\frac{dT}{dt} + \dot{Q}_c + \dot{Q}_e \tag{3}$$

where

$$\dot{Q}_c = \pi d \frac{\mu_f}{\mathrm{Pr}_f} c_{p,f}(T_g - T_d)\left[2 + \frac{k}{F(B_t)}\mathrm{Re}^{1/2}\,\mathrm{Pr}_f^{1/3}\right]\frac{\ln(1+B_t)}{B_t}$$

$$\dot{Q}_e = -\dot{m}h_{v,f}$$

In these expressions, $\mathrm{Pr}_f = \nu_f/\alpha_f = c_{p,f}\mu_f/k_f$ is the film Prandtl number and hv,f is the heat of vaporization. A "thin-skin" model is used and conditions at the droplet surface are obtained iteratively by equating heat flux to the droplet with droplet heating and enthalpy associated with vaporization [67]. The relationship between the quasi-steady-state film temperature and the fluxes to the droplet are modeled by the Spaulding heat transfer number, $B_t = [1 + B_m]^{1/\mathrm{Le}_f} - 1$.

The thermodynamic properties at the droplet film surface are obtained by using a thin-skin approximation [67], where the film temperature is approximated as a weighted average of the droplet and surrounding gas temperatures, $T_f = \alpha T_g + (1-\alpha)T_d$. In this study, the weighting function, α, is set to a fixed value such as $\alpha = 1/3$, leading to the so-called "1/3 rule" [26]. The film is assumed to be at saturation conditions so that a partial pressure can be calculated using a Clausius–Clapeyron relation as

$$P_{\text{sat}} = P_{\text{atm}} \exp\left[\frac{h_v}{R}\left(\frac{1}{T_{\text{ref}}} - \frac{1}{T_f}\right)\right] \tag{4}$$

where the heat of vaporization, h_v, is expressed as a function of temperature using Watson's relation [34],

$$h_v = h_{v,\text{ref}}\left[\frac{T_{\text{crit}} - T_f}{T_{\text{crit}} - T_{\text{ref}}}\right]^{0.38} \tag{5}$$

where T_{crit} and T_{ref} are the droplet critical and reference temperatures, respectively. Once the saturation pressure is determined, the mass fraction of water vapor is calculated from the ideal equation of state as

$$Y_f = \frac{MW_{H_2O}}{MW_g}\left[\frac{P_g}{P_{\text{sat}}} - 1 + \frac{MW_{H_2O}}{MW_g}\right] \tag{6}$$

The mass and thermal transfer numbers (i.e., B_m and B_t) are obtained from their definitions as derived from steady-state droplet analysis using $B_m = (Y_f - Y_g)/(1 - Y_f)$ and $B_t = [1 + B_m]^{1/\text{Le}_f} - 1$.

Fire Suppression Model

Within VULCAN [68], chemical reactions are greatly simplified, reflecting the predominance of mixing processes in fires. This simplified treatment of kinetics is not sufficient for suppression predictions, and suppression criteria are determined by employing a subgrid scale suppression model [30]. The VULCAN suppression model is based on the concept of a critical Damkohler number for extinction, where the Damkohler number represents the ratio between the chemical and fluid mixing time scales. This captures the physics of both oxygen depletion and cooling of the flame in fire suppression because both act to increase the chemical time scales. The chemical time scales are determined by conducting a series of computations of the blow-out limits for a perfectly stirred reactor (PSR). The PSR approximation

is consistent with the subgrid EDC combustion model, which treats the mixture distribution as discrete delta functions for the flame zone and surroundings; effectively, a Le = Sc = 0 approximation within the flame zone. The PSR results are precalculated using the CHEMKIN II [69] software package PSR module [70]. This chemical time scale, the PSR blow-out time scale, is parameterized as a function of the suppressant-reactant mixture composition and temperature. The fluid time scale is taken to be the Kolmogorov time scale based on standard turbulence theory, $\tau_K = 0.41(\nu/\varepsilon)^{1/2}$, where ν and ε are the molecular viscosity and the turbulent kinetic energy dissipation. The Damkolher number is then the ratio of this fluid time scale to the chemical time scale, determined from the PSR calculations; and for Damkohler numbers below a critical value, the flame is locally extinguished, and the source terms in the code are set to zero. The critical Damkohler number for extinction was determined from jet blow-off studies [71] to be 1.367, and is thus independent of the suppressant. A similar criterion for flame extinguishment has been recently used by Koutmos [72] for LES, but the Damkohler number comes from a dynamic length scale ratio rather than being constant.

For mixtures of suppressants, mixing rules are used that allow the mixture mole fraction of suppressant to be determined using the following expression:

$$\frac{1}{X_{LIM_{\text{mix}}}} = \sum_{\text{species}} \left[\frac{X_{\text{relative}}}{X_{LIM_{\text{species}}}} \right] \tag{7}$$

where $X_{LIM_{\text{species}}}$ is the suppressant mole fraction that extinguishes the flame for a specific suppressant species, X_{relative} is the mole fraction of that particular suppressant species divided by the total suppressant mole fraction, and $X_{LIM_{\text{mix}}}$ is the suppressant mole fraction for extinction for the suppressant mixture. These mixing rules work for suppressants that are mostly thermal in nature and are therefore well suited for studying the effects of water on flame suppression, but also allow the joint consideration of agents like CO_2 or even halofluorocarbons.

MODEL EVALUATION

It is necessary to show the performance level of the current model by comparing the numerical prediction of the model against experimental data. In this section, the fire scenario of Chow et al. [50] is chosen for our comparison study. In that experiment, a local gas temperature history was recorded

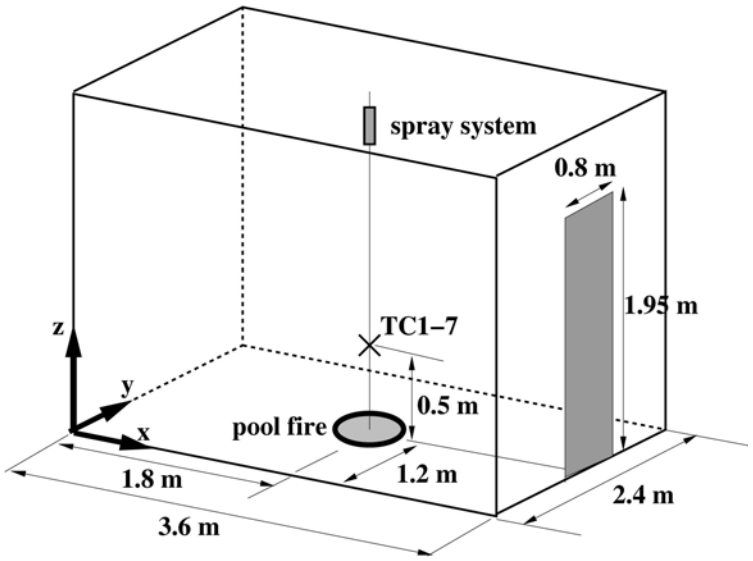

Fig. 2 Schematics of the experimental setup of Chow et al. [50].

using a thermocouple (TC1-7) located at 0.5 m directly above the gasoline pool fire (0.5 m diameter) as shown in Fig. 2. Full ignition of the 0.5 m diameter fire took about 8 s. The water spray was injected at t = 60 s, the time at which the fire was at quasi-steady state. Data was recorded up to t = 400 s. The mean droplet size of the commercial water spray was about 340 μm. The total mass flow rate was $\dot{m} = 0.02$ kg/s.

In the simulations, the droplet injection speed was varied (within the range 0.2 m/s < U_{inj} < 52 m/s) since this information was not reported by Chow et al. [50], while the mean droplet size and mass flow rate were taken from their paper. The time step used for the gas-phase simulation was $\Delta t_{\text{gas}} = 0.1$ s while the subcycling time step for the liquid phase was around $\Delta t_{\text{spray}} \approx \Delta t_{\text{gas}}/100$ s, set by the stability criterion implemented in the fire suppression code with the given maximum injection speed of the water spray. The computational mesh was 110,400 nodes (60 × 46 × 40) with refined grid resolution around the pool fire to better capture the detailed interaction between the water droplets and the flame surface region. The cone angle of the spray was set as θ = 60 deg and the spray injection was initiated at t = 60 s, consistent with the experimental operating conditions of Chow et al. [50]. The initial droplet size distribution was assumed to be the Rosin-Rammler distribution shape [i.e., PDF(D) = $(qD^{q-1}/X^q)\exp[-(D/X)^q]$, where D is the droplet diameter and X is the characteristic droplet size] with the corre-

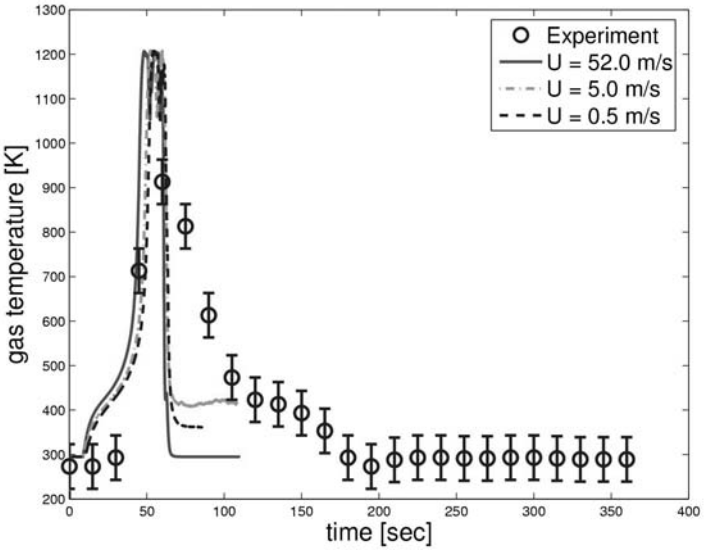

Fig. 3 Time evolution of the local gas temperature at x = 1.8 m, y = 1.2 m, and z = 0.5 m (TC1-7 location). Spray injection is initiated at t = 60 s and stops at t = 400 s.

sponding dispersion coefficient of q = 3, deduced from the measurement obtained for a typical commercial water sprinkler according to Widmann [73].

The local gas temperature measurement was taken at the location denoted TC1-7 (see Fig. 2). The temperature history there is shown in Fig. 3 and is compared to the computational predictions. As shown in Fig. 3, it took about 60 s to reach the maximum value, T_{gas} = 913 K. Predicted higher values of temperature may be due to heat losses to the wall surfaces that are not accounted for in the current study where the walls are assumed to be adiabatic.

Three droplet injection speeds, U_{inj} = 0.5, 5, and 52 m/s, are considered in order to study their effect on suppression. In all cases, suppression was achieved with a high mass flow rate of water, $\dot{m} = 0.2$. However, a moderate temporary increase in the gas temperature is observed for U = 5.0 m/s, probably because of the enhanced turbulent mixing induced by the spray injection. The computation was stopped at around $t \sim 100$ s; no further calculation was possible due to high computational cost. From this comparison in Fig. 3, it is observed that the model generally overpredicts the suppression efficiency, compared with the experimental data for most cases. The comparison would have been more insightful if the exact injection speed used in the experiment were known. The suppression behavior or its history

is somewhat different depending on the injection speed, except for the fact that they all eventually result in suppression. This comparison qualitatively shows that the model will predict the suppression condition (whose results are comparable to that of the experiment), which is satisfactory at the current stage of the research. In the future, more accurate quantitative comparison would be desired for the purpose of code validation.

THE EFFECT OF DROPLET MOMEMTUM ON SUPPRESSION

In this section, we discuss parametric studies on a large-scale pool fire placed in a 2 m × 2 m square burner at the center of a floor in a 10 m × 10 m × 10 m compartment with an open ceiling, as depicted in Fig. 4. To the authors' knowledge, scientific fire suppression studies at this large scale have not been conducted, either experimentally or numerically. Figure 4 also shows the coordinate system used in all of the following discussion.

A direct comparison with experimental data has not been made due to the lack of experimental data for a large-scale compartment fire. Table 5 lists the parameters covered in this study. It is expected that suppression is achieved for most parametric cases due to the high mass flow rate applied for the water-spray system, $\dot{m} = 5$ kg/s. Thus, we here define that the opti-

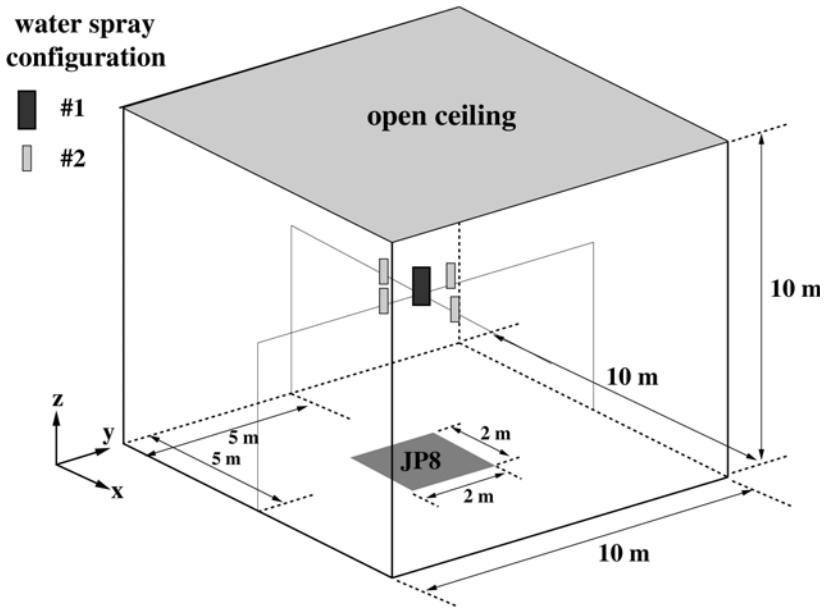

Fig. 4 Schematics of the compartment fire of the modeling.

Table 5 Parametric Case Studies Conducted During the Simulations

Case No.	X (μm)	U_{inj} (m/s)	Config. No.
1	200	20	1
2	200	40	1
3	200	80	1
4	400	20	1
5	400	40	1
6	400	80	1
7	800	20	1
8	800	40	1
9	800	80	1
10	100	80	1
11	200	80	2

mum fire suppression condition is found when the selected local flame temperature is reduced to a room temperature of 300 K at the fastest rate with respect to other cases, for a fixed water mass flow rate.

Computational Details

The water spray is injected from the center of the cube-shaped room, at $x_{inj} = y_{inj} = z_{inj} = 5.0$ m, and the droplet velocity was varied from $U_{inj} = 20$ m/s to 80 m/s. The time step used for the gas-phase simulation was $\Delta t_{gas} = 0.05$ s while the subcycling time step for the liquid phase was approximately $\Delta t_{gas} \approx \Delta t_{gas}/100$ s, set by the stability criterion implemented in the fire suppression code with the given maximum injection speed. A uniformly spaced grid was applied with a resolution of 132,651 nodes (51 × 51 × 51). The cone angle of the spray was set at $\theta = 30$ deg and the spray injection was initiated at $t = 20$ s. Statistics on the spray characteristics were collected at intervals of 0.002 s, from $t = 25$ s through 30 s (2500 data points). The total number of computational parcels injected was 50,000 parcels during a 10 s spray injection duration (or 5000 parcels/second). The total number of water droplets ranged from 186 million to 12 billion, which yielded an average value of $\sim 3.72 \times 10^3$–2.4×10^5 droplets/parcel. The initial droplet size distribution was assumed to be the Rosin–Rammler distribution shape with the corresponding dispersion coefficient of $q = 3$, deduced from the measurement obtained for a typical commercial water sprinkler according to Widmann [73].

Quasi-Steady State of the Hydrocarbon Pool Fire

As indicated earlier, the water spray was initiated at t = 20 s, when the pool fire reached a quasi-steady state. In Fig. 5, the local gas temperature is shown for various physical locations. The solid and dashed lines correspond to the physical locations x = 1.7 and 5.0 m, respectively, which is off and on the centerline. The legends ○, ×, and * represent the vertical locations, z = 2, 4, and 6 m, respectively. As shown, the dashed line data are higher because they were located directly above the pool fire at x = 5.0 m. It is also evident that the location closest to the pool in the vertical direction (i.e., x = 5 m and z = 2 m) has the highest temperature. As the height increases from 2 to 6 m, the temperature decreases above the fire at x = 5.0 m due to increased air entrainment. Away from the fire at x = 1.7 m, the opposite trend occurs with the temperature increasing with height, corresponding to the buoyantly stable hot upper layer gases recirculating in the downward direction as they cool.

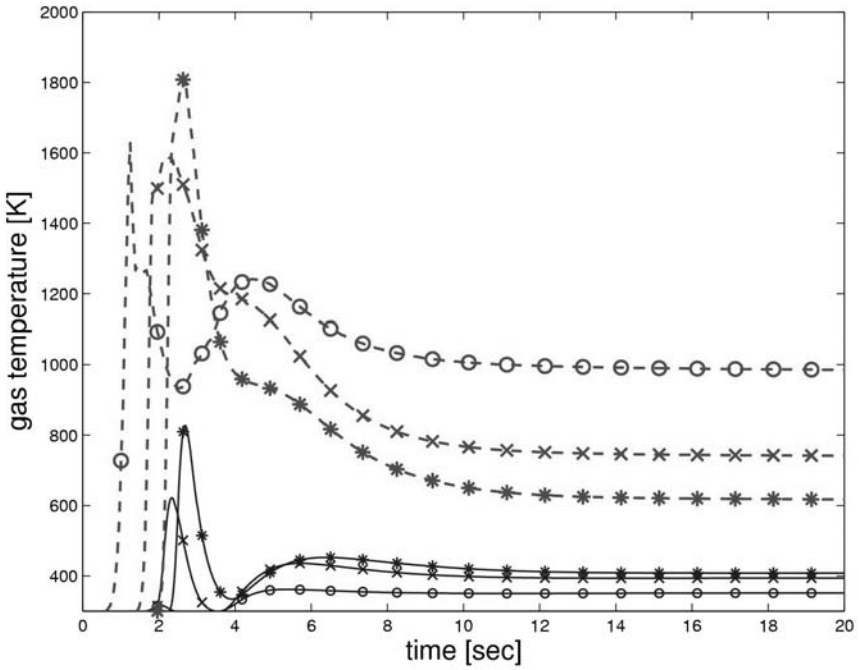

Fig. 5 Time evolution of the local gas temperature at various physical locations at the y = 0 plane. The solid and dashed lines correspond to x = 1.7 and x = 5.0 m, respectively. The legends ○, ×, and * represents the vertical locations, z = 2, 4, and 6 m heights, respectively. A quasi-steady state is reached at about t = 10 s. Note that spray injection is initiated at t = 20 s and stops at t = 30 s.

The stationary room temperatures indicate that the fire has reached a quasi-stationary state prior to the injection of the water spray at 20 s.

From this basic configuration, a parametric study of the key variables that determine the effectiveness of a water-spray fire suppression system is conducted. These variables include the droplet size and the droplet momentum. These are varied to study the experimental observations that water mist systems, those with small droplet diameters, are extremely effective fire suppression systems *if* the water mist can get to the fire. The problem arises in getting to the fire because the momentum of the individual droplets is not sufficient to penetrate the fire, the upward buoyant flow tending to push them away. Instead, the momentum of the entire spray plays a role in determining the effectiveness when the momentum of the individual drops is not sufficient. These trade-offs are addressed in the following sections. The issue of the number of nozzles is also addressed. For all of these cases, the fire and the water mass flow rate are held constant. The conditions for the various tests are detailed in Table 5. The results for varying droplet size are presented first, followed by the variations in the spray momentum.

Effect of Initial Droplet Size

In Fig. 6, a series of snapshots of the water spray, with the droplet injection speed fixed at 20 m/s, is shown for various initial droplet sizes: X = 200, 400, and 800 μm (cases 1, 4, and 7; see Table 5). The smaller droplets decelerate rapidly and are subject to more rapid evaporation, and the smallest droplets from all three of these cases are observed to be lofted upward by the buoyant fire plume. These droplets do not approach the fire closely enough to effectively suppress the fire. This failure is particularly apparent for case 1 with X = 200 μm. Suppression in this case is delayed until the water droplets are recirculated by the convective flow. Figure 7 shows the suppression phenomenon for X = 200, 400, and 800 μm. At t = 22 s, suppression was not achieved for X = 200 μm. However, a gradual improvement in the suppression condition is clearly shown in Fig. 7, and complete suppression is shown for X = 800 μm.

Contour plots for the time-averaged Sauter mean diameter (SMD) are shown in Fig. 8 for X = 200, 400, and 800 μm. As seen in Fig. 8a, droplets larger than about 500 μm actually landed on the floor (z = 0), where the pool fire was located. When the injected droplet size increases, the shape of the spray envelope becomes more apparent because these larger droplets maintain their initial momentum more efficiently. The size distribution for X = 800 μm in Fig. 8c is such that large droplets (i.e., $D \sim$ 1200 μm, the dark

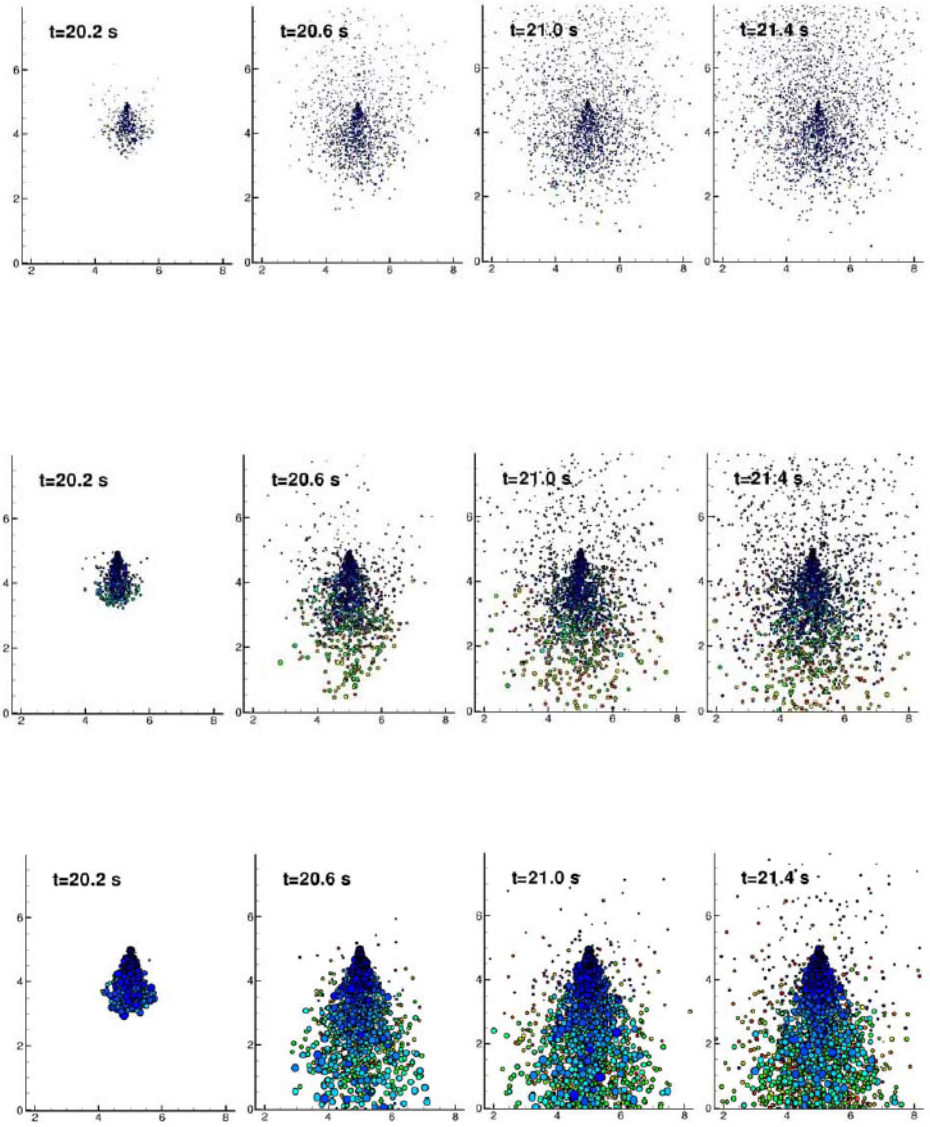

Fig. 6 Time evolution of spray injection at U_{inj} = 20 m/s in the x–z axes frame (y = 0 plane), (first row) X = 200 μm, (second row) X = 400 μm, and (third row) X = 800 μm (cases 1, 4, and 7). Small droplets are lifted upwardly due to the buoyancy force of the pool fire, whereas large droplets have enough momentum to penetrate into the fire located at the bottom. The contour color is scaled with the axial velocity of the droplets.

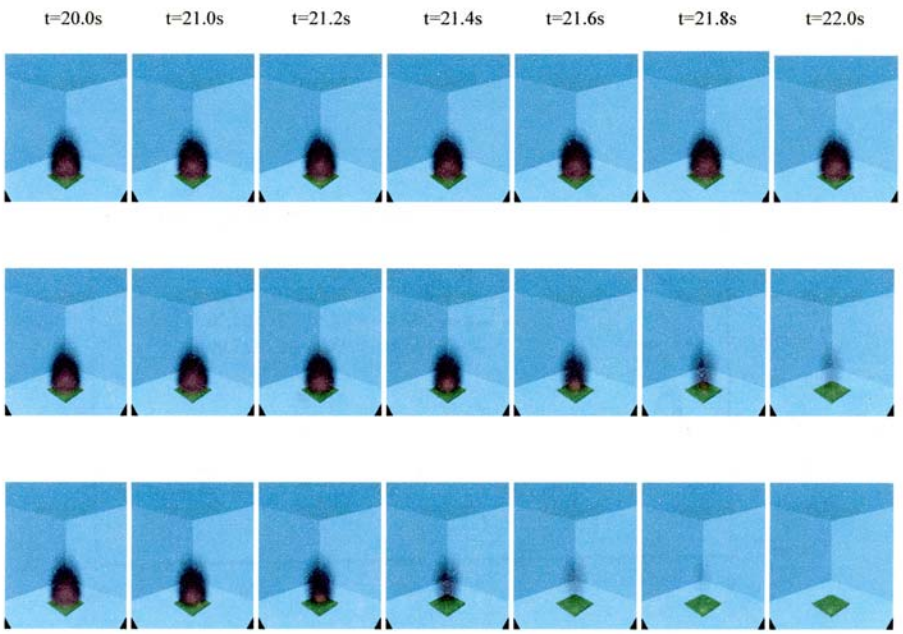

Fig. 7 Time evolution of fire suppression of a hydrocarbon pool fire for (first row) X = 200 μm, (second row) X = 400 μm, and (third row) X = 800 μm. Note that the spray injection speed is U_{inj} = 20 m/s (cases 1, 4, and 7).

column in the center) were projecting directly in a downward direction while smaller droplets were located between the center column and the edge of the spray envelope. Figure 9 shows the time-averaged radial gas velocities near the pool surface (z = 0.25 m) are plotted to show the extent to which the spray momentum is transmitted toward the pool surface. As the spray penetrates the upper regions of the fire, a stagnation flow pattern is generated with the radial outflow indicated in Fig. 9. This radial outflow is substantially stronger with the greater initial droplet diameter. In addition to the effectiveness of the droplets in cooling the fire, the stagnation flow can push the fire outward, reducing the view factor between the fire and the pool; this reduces the heat flux to the pool and thus the strength of the fire, as also observed by Chow et al. [50].

To enhance the effectiveness of smaller droplets, it is hypothesized that increased spray momentum can lead to better mixing of the droplets into

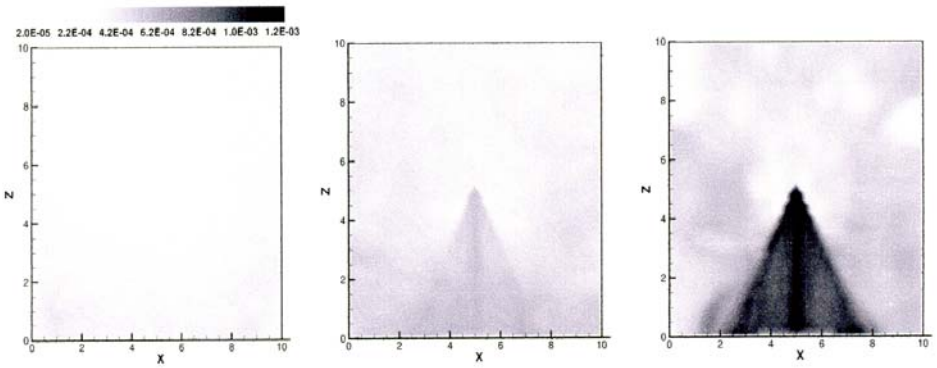

(a) X = 200 μm (b) X = 200 μm (b) X = 200 μm

Fig. 8 Time-averaged Sauter mean diameter, D_{32}, distribution in x–z coordinates (y = 0 plane) at various injection mean diameters, X = 200, 400, and 800 μm. Note that the spray injection speed is U_{inj} = 20 m/s (i.e., cases 1, 4, and 7) and the contour level is scaled with D_{32} in the unit of m.

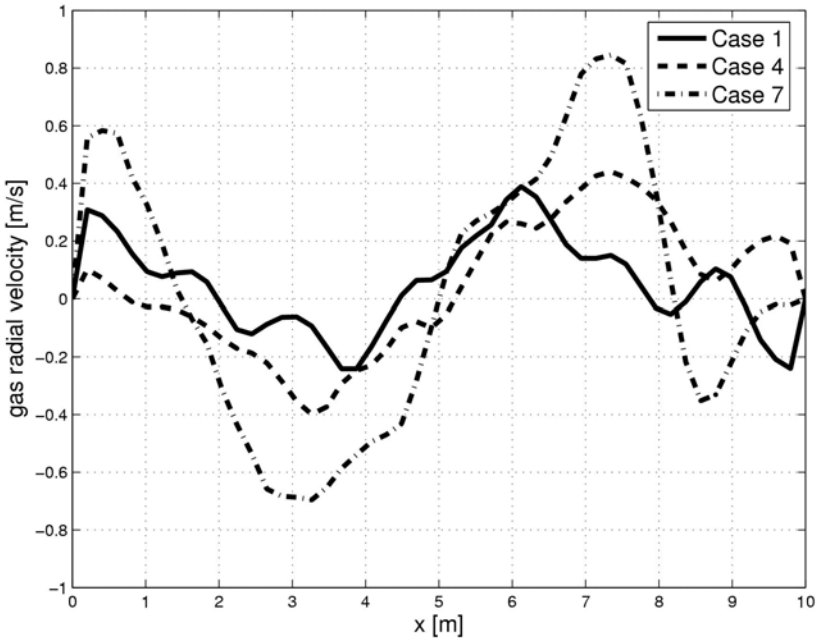

Fig. 9 Time-averaged gas radial velocities near the fuel surface (i.e., z = 0.25 m) for X = 200, 400, and 800 μm (i.e., cases 1, 4, and 7). A stronger radial velocity is shown for larger mean droplet size, although droplets were injected at the same speed for all cases.

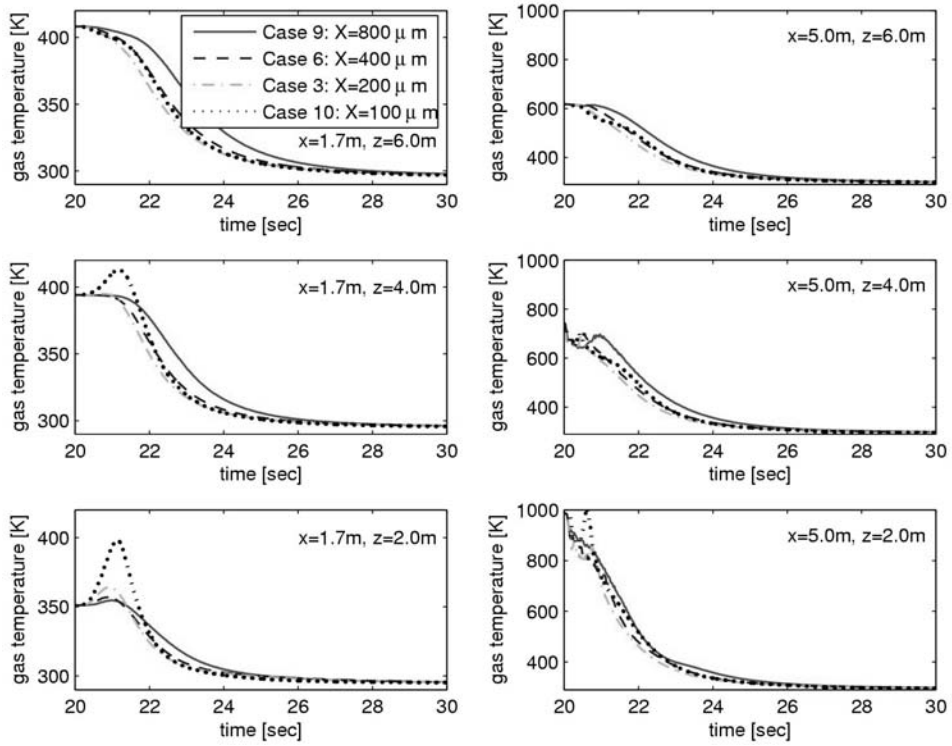

Fig. 10 Comparison of the time history of the local gas temperature for cases 9, 6, 3, and 10 (X = 800, 400, 200, and 100 μm) under the spray injection speed, U_{inj} = 80 m/s.

the fire. Therefore, the effect of droplet size is also examined for higher initial droplet velocities. These cases, with initial droplet velocities of 80 m/s, and initial mean diameters from X = 800 μm to X = 100 μm are denoted as cases 9, 6, 3, and 10, in order of decreasing droplet diameter, in Table 5. These results are shown in Fig. 10. Here, the greater momentum of the spray enhances the mixing so that the temperature drops off more rapidly than in those cases discussed in Figs. 6–8. However, the effect of reduced droplet diameter on enhancing the suppression is small. That is, there is a low sensitivity to the droplet diameter at sufficiently high initial velocities. Furthermore, for the smallest (X = 100 μm) droplets, there is some evidence of marginally higher temperatures with smaller diameters. This implies that the droplet

evaporation may be too fast for these large scales, although we suggest that additional work would be required to validate this.

Effect of Spray Injection Speed

The well-known behavior in which smaller droplets have difficulty suppressing a fire because the individual low-momentum droplets are unable to penetrate the buoyant plume was described in the previous section. In the present section, the injection speed is varied to determine the effect of the overall spray momentum in mitigating the above-mentioned small-droplet disadvantage.

Figure 11 shows the gas temperature contours at t = 30 s for various injection speeds, U_{inj} = 20, 40, and 80 m/s, under a fixed initial droplet size of X = 400 μm (cases 4–6). For U_{inj} = 20 m/s, the maximum gas temperature was around 345 K and thus complete suppression was not achieved. The stagnation zone, where the downward motion of the spray and the upward motion of the buoyant fire met, was slightly below the spray location, $z \sim$

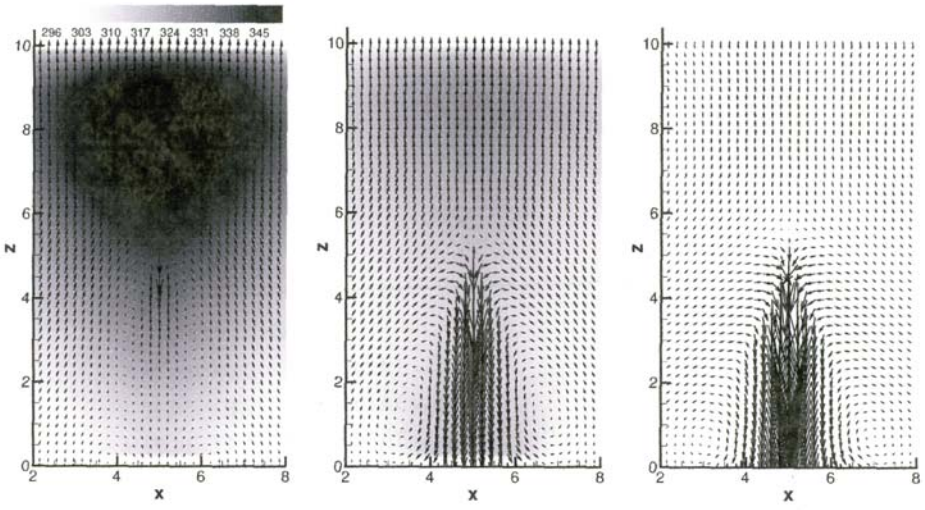

(a) U_{inj} = 20 m/s (b) U_{inj} = 40 m/s (c) U_{inj} = 80 m/s

Fig. 11 Effect of varying the injection speed on the induced local gas velocities and on the suppression mechanism; the suppression is enhanced as the injection speed increases. Contour color is scaled with the local gas temperature at t = 30 s. Note that the initial mean droplet size is X = 400 μm (i.e., cases 4–6).

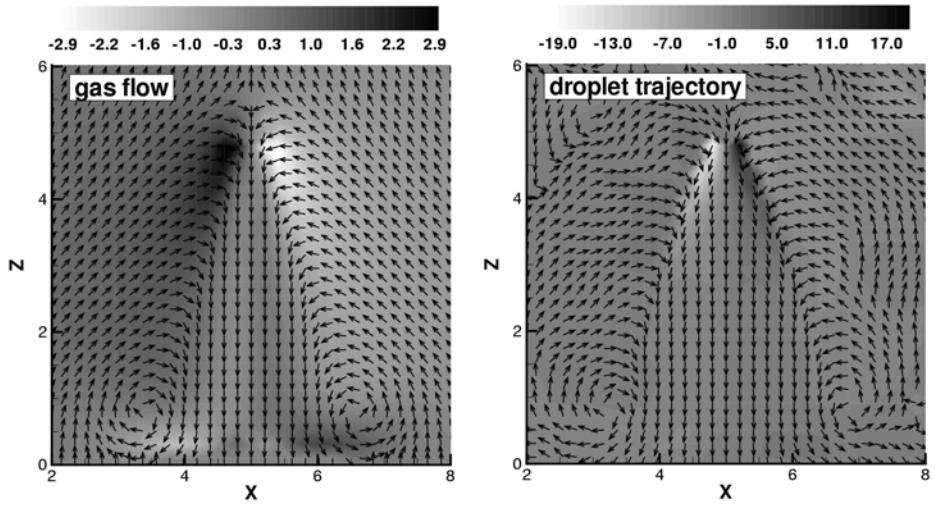

Fig. 12 Time-averaged (a) induced gas and (b) injected droplet velocities for case 3, X = 200 μm and U_{inj} = 80 m/s. Vortex roll up is shown near the floor surface (i.e., z = 0); the induced gas is radially convected. Contour color is scaled with the radial velocities of (a) gas and (b) droplet in the units of m/s. Note that the vectors are plotted at uniform length for clarity of the presentation.

4.0 m (see Fig. 11a). As the injection speed increased, the stagnation zone was pushed downward, to $z \sim 4.0$ m for the U_{inj} = 40 m/s case. Eventually, the zone stopped at $z \sim 1$ m for U_{inj} = 80 m/s for the case where complete suppression was achieved. From this observation, we may conclude that the stagnation zone location is a good measure to provide information regarding suppression conditions. As seen in Fig. 12, the stagnation zone was clearly located near the floor surface, indicative of the strong momentum of the spray droplets that overcame the buoyant force of the fire. Certainly, the spray droplet trajectory induced the motion of gas flow, which is similar in motion to the droplet as shown in Figs. 12a and 12b.

In Fig. 13, the history of the local gas temperature is shown at various physical locations for cases 1, 4, and 7, where droplet size was varied. Figure 13 indicates that the largest droplet size resulted in the smallest time to suppression when the injection speed was relatively low (U_{inj} = 20 m/s). This pattern was true for all six physical locations as shown in Fig. 13.

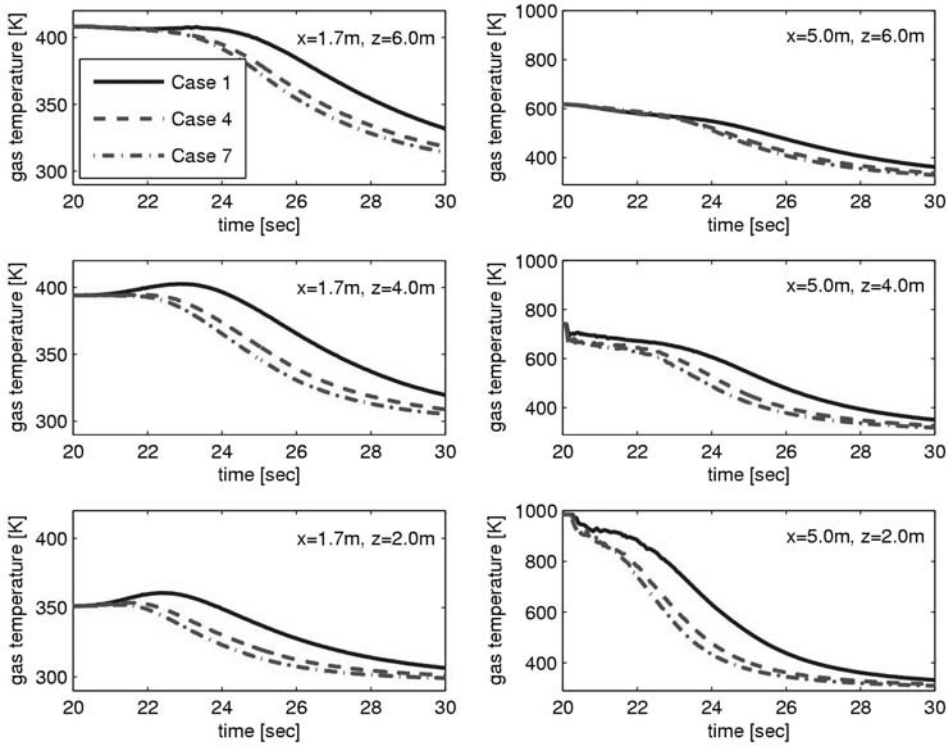

Fig. 13 Comparison of the time history of the local gas temperature for cases 1, 4, and 7 under the spray injection speed U_{inj} = 20 m/s. Note that the range of the gas temperature for the left panes (x = 1.7 m) is up to 420 K, while that for the right panes (x = 5.0 m) is up to 1000 K.

Sensitivity of Suppression to Droplet Size and Initial Velocity

In order to quantitatively assess the significance of the above results, the sensitivity of the suppression time to the droplet size and initial velocity are now computed. Here,the suppression time is defined as the time for the temperature at the position $x = y = 0.5$ m and $z = 0.4$ m to be reduced to 350 K (see Fig. 14). The suppression time sensitivity is then defined as

$$S_X = \frac{d \ln (t_s)}{d \ln (X)} \quad \text{and} \quad S_{U_{\text{inj}}} = \frac{d \ln (t_s)}{d \ln (U_{\text{inj}})} \tag{8}$$

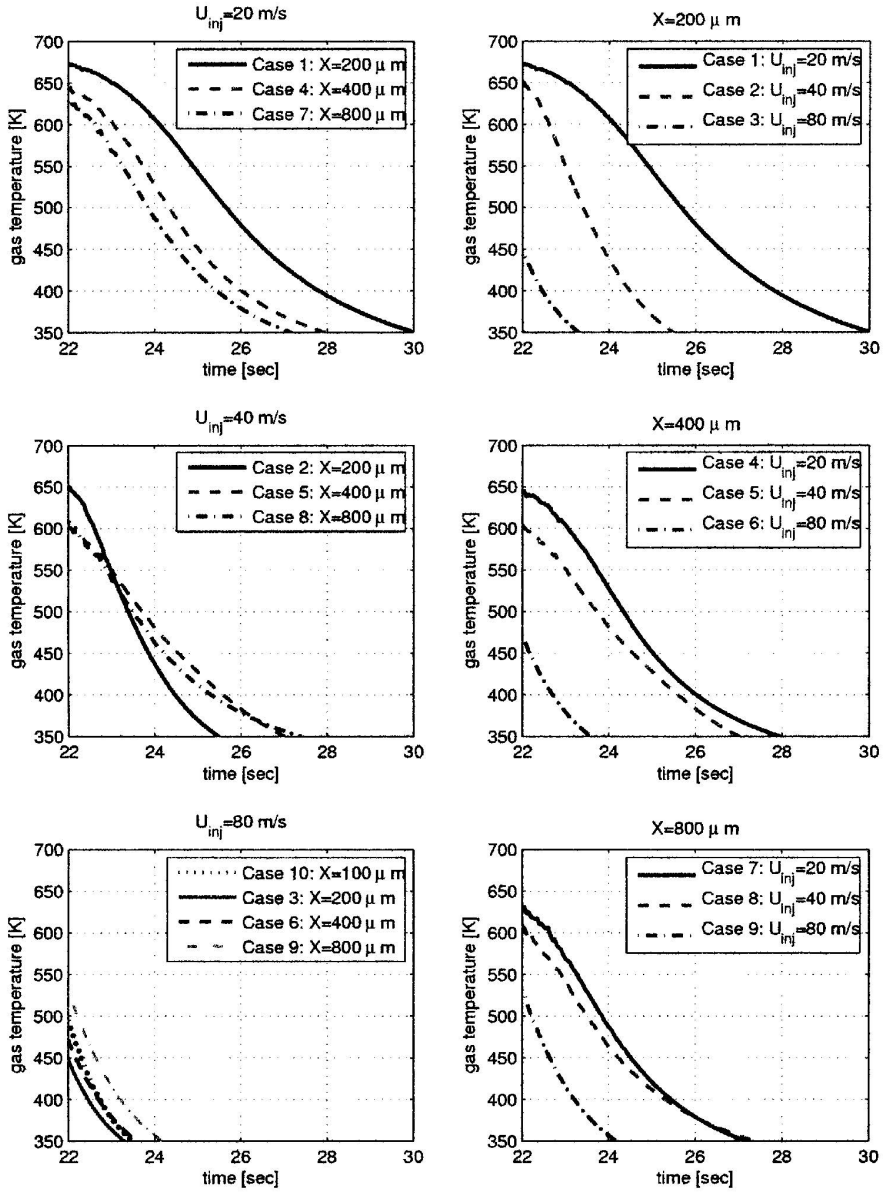

Fig. 14 Comparison of the time history of the local gas temperature for cases 1–9 at the physical location $x = y = 0.5$ m and $z = 0.4$ m.

which are the fractional changes in the suppression time for a given fractional change in the droplet mean diameter and initial velocity, respectively. A positive sensitivity indicates that increasing X (or U_{inj}) results in a longer time to suppression; in this sense, positive sensitivities indicate a system that would be optimized by reducing X (or U_{inj}). Sensitivities are computed by finite differences between the conditions in Table 5 so that sensitivities are identified by the range of X or U_{inj} over which they are computed. For example, the sensitivity to velocity computed between the middle and larger velocity is denoted by 40–80 m/s. These values are shown in Fig. 15, where several distinct trends discussed in previous sections can be quantified.

The suppression-time sensitivity exhibits a complex behavior that reflects the existence of various regimes. If we start by considering the sensitivity to the droplet diameter at low initial droplet velocities (see the U_{inj} = 20 m/s case from Fig. 15a), the negative sensitivity that grows for smaller droplets reflects the fact that there is insufficient momentum in the spray to push small droplets into the fire. In this case, the larger droplets with a greater ability to penetrate the fire are more effective. Furthermore, because they have difficulty penetrating the fire, small droplets have a relatively high sensitivity (larger deviation from $S_x = 0$) at these low flow rates.

For larger initial droplet velocities, the sensitivities switch to positive, indicating that the spray momentum is strong enough to take advantage of the small droplets' rapid evaporation rates. Furthermore, as the momentum of the spray increases, the magnitude of the sensitivity to droplet size for the smaller droplets is reduced further. For the smallest droplets (X = 100 μm), the sensitivity switches again to negative, indicating that these droplets are probably evaporating early, but the magnitude of the sensitivity is still small. This information is valuable for applications because it indicates that a wide range of droplet sizes are permissible if the spray momentum is strong enough.

Considering now the sensitivity to the initial droplet velocity (see Fig. 15b), it is seen that strong negative sensitivities exist for higher velocities. That is, increasing the velocity increases the mixing rates and results in faster suppression. This behavior occurs for the full range of velocities with the smallest droplets since they are largely dependent on the momentum of the full spray, but the sensitivity is reduced for large particles at lower velocities since larger particles can take advantage of their own momentum to penetrate the fire. We note here that the insensitivity of large particles is somewhat dependent on the relative locations of the nozzle and fire since the scope of the spray is primarily limited to the spray cone with the large particles, as indicated in Fig. 8.

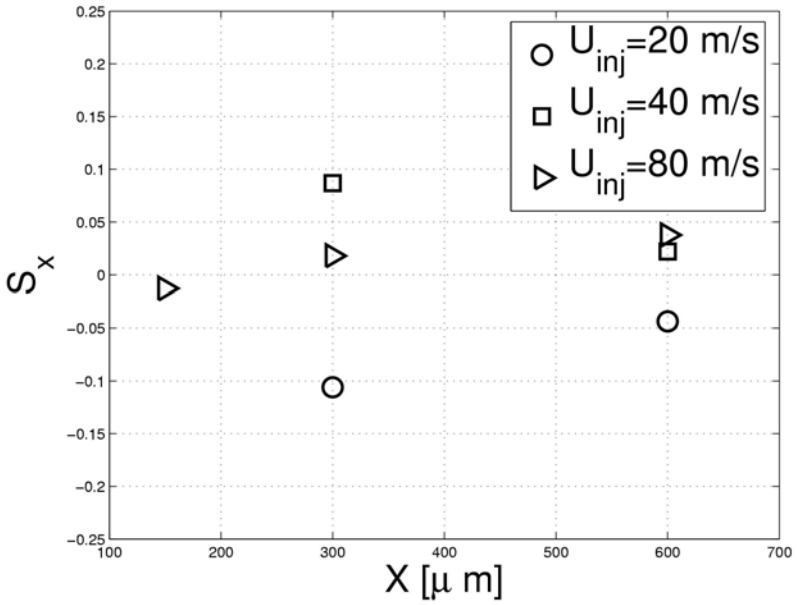

(a) Effect of initial injection speed

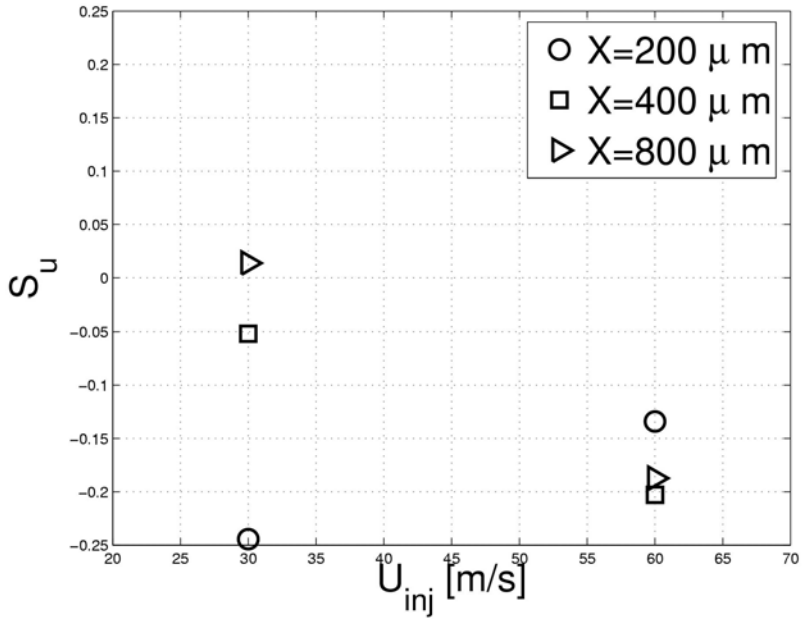

(b) Effect of initial droplet size

Fig. 15 Sensitivities (S_x and S_u) due to the initial droplet size and speed.

Effect of Spray Configuration

A single nozzle positioned directly over a fire maximizes the spray penetration into that fire. In general, ceiling mounted water-spray systems are placed in arrays to achieve area coverage of a room. The worst configuration is, then, having the fire positioned equidistant from four nozzles, thus minimizing the vertical momentum of the spray jets against the fire. To demonstrate this effect, an additional parametric study (case 11) is conducted regarding the change in spray configuration (see Fig. 3). Configuration 2 (as in Fig. 3) was set up so that four nozzles were installed at a 0.5 m distance away from the center point of spray configuration 1, in the east, west, south, and north directions. Each nozzle delivered a mass flow rate of $\dot{m} = 1.25$ kg/s, one quarter the total mass flow rate used in configuration 1. The injection speed remained the same as in case 3 (U_{inj} = 80 m/s) and, thus, it is supposed that the nozzle diameter was reduced because the mass flow rate was reduced for configuration 2.

In Fig. 16, the gas local temperature from case 3 (configuration 1) and

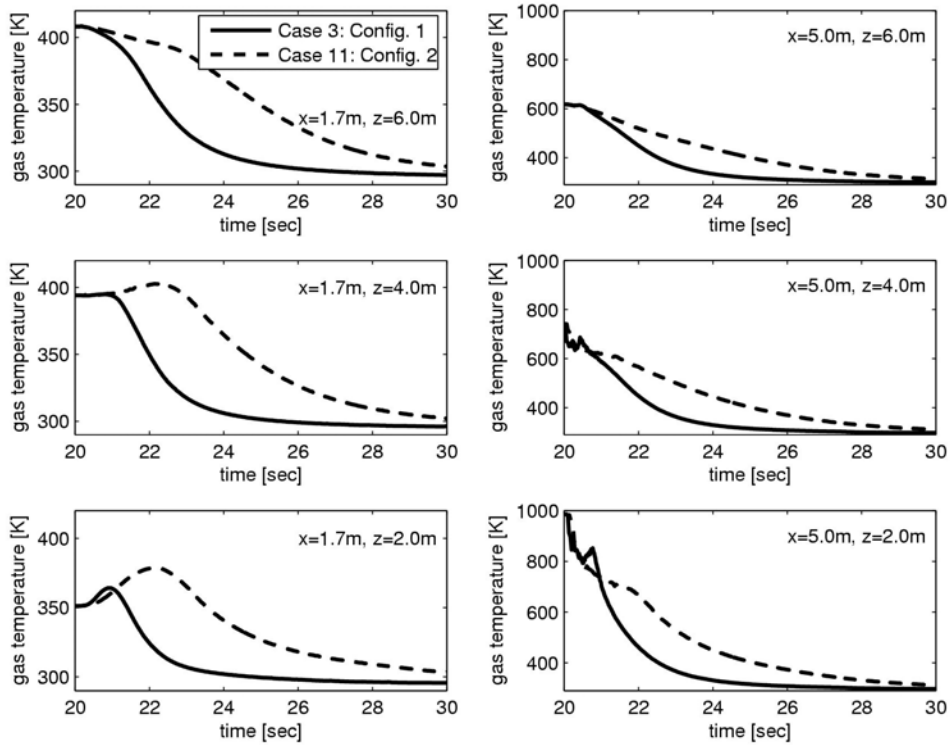

Fig. 16 Comparison of the time history of the local gas temperature for case 3 (configuration 1) and case 11 (configuration 2) under the spray injection speed U_{inj} = 80 m/s.

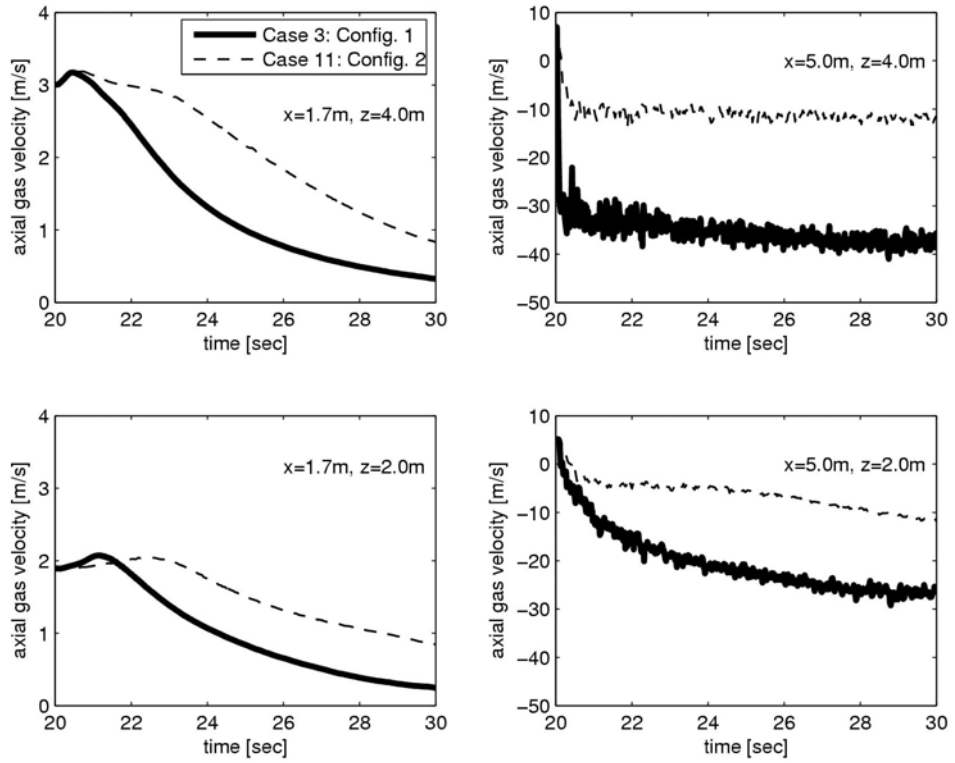

Fig. 17 Comparison of the time history of the local gas axial velocities for case 3 (configuration 1) and case 11 (configuration 2) under the spray injection speed U_{inj} = 80 m/s.

case 11 (configuration 2) is compared. The temperature reduction rate became smaller when using four nozzles in a configuration and, therefore, configuration 2 was found to be less efficient in suppressing the fire. The spray system with four nozzles induces a greater turbulent mixing between the fire and the air, resulting in a larger increase in the local gas temperature. The penetration of the spray was less efficient for the four-nozzle configuration, as shown in Fig. 17. The higher location of the stagnation zone shown in Fig. 18 was another indication that the four-nozzle configuration was a poor spray suppression system as compared to the one-nozzle configuration. The overall spray momentum from the four-nozzle setup was less efficient in that droplets were lifted upward due to the fire buoyancy force and never reached the surface of the fuel at the floor. It should be noted that this observation is limited to the case with a single fire in an open room. If the fire

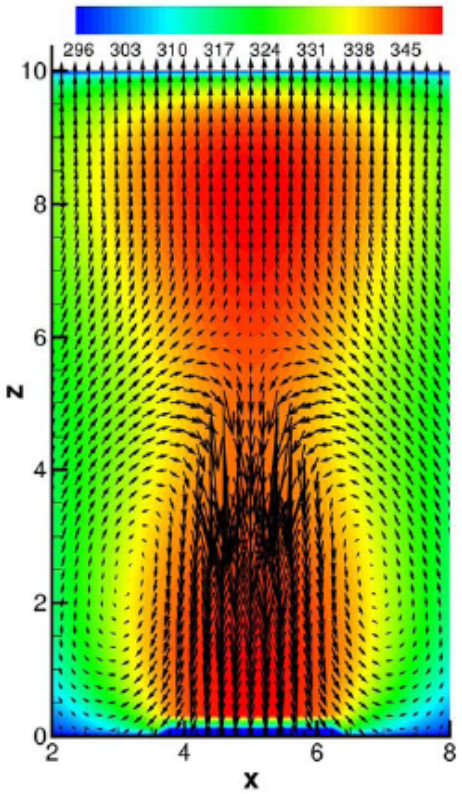

Fig. 18 The induced local gas velocities during four-nozzle injections (case 11); combustion is enhanced due to the intensified turbulence mixing of the larger vortex roll-up motion. The contour color is scaled with the local gas temperature at t = 27 s.

is obstructed by surrounding objects from the spray nozzles, then the same conclusions cannot necessarily be drawn.

From these results, it is clear that if a suppressant is to be delivered against the buoyant momentum created by a fire, then spray momentum is an important parameter. It has long been known that much of the air entrained into the fire occurs at the base of the fire (see, for example, [74]). If water mist is supplied at the base of the fire, it will not need to overcome the fire momentum, but will be drawn into the fire by the entraining air. Hence, the often quoted rule of handheld fire extinguisher use to point the extinguisher at the base of the fire (and sweep to cut off the oxygen supply).

Ceiling mounted sprinklers are not clearly optimal suppression devices if the location of the fire is known, since the spray must overcome the fire

momentum. However, they are well suited for their intended use as area coverage devices for fires that may occur at any location along the floor, walls, or ceiling, provided that the ceiling is not too high, as in tall atriums [75].

CONCLUSIONS

The effect of the average droplet size and the droplet initial velocity in the water-spray suppression of a large-scale JP8 compartment pool fire was studied using the VULCAN suppression model. Comparisons between existing experimental data and the VULCAN predictions showed consistency between the predictions and measurements. A computational study was also conducted to investigate the dependence of the time to suppression on the droplet diameter and initial velocity. This computational study indicates that higher injection velocities are generally associated with more rapid suppression. This trend is particularly true for smaller initial droplet diameters that tend to be very effective in suppressing fires if they can be transported into the fire. In this sense, it is observed that an optimal suppression system would operate with small droplets at high initial velocities. For droplet distributions with sufficiently small average diameters, the rate of suppression is relatively insensitive to the droplet size, indicating that additional effort in making smaller or more uniform droplet sizes is unwarranted. For lower initial velocities, however, smaller droplets have trouble penetrating the fire and are relatively ineffective. For the conditions evaluated, a four-nozzle configuration seemed to be less efficient than the one-nozzle configuration; the spray system with four nozzles induces a greater turbulent mixing between the fire and the air, resulting in a temporary increase in the local gas temperature. The penetration of the spray was less efficient for the four-nozzle configuration. The location of the stagnation zone between the downwardly injecting spray and the upwardly lifting fire plume was found to be an important parameter for the consideration of the preferred suppression condition.

ACKNOWLEDGMENTS

This work was supported by the Defense Threat Reduction Agency (DTRA) and was performed by Sandia National Laboratories (SNL), a multiprogram laboratory operated by Sandia Corporation, a Lockheed Martin Company, for the United States Department of Energy's National Nuclear Security Administration under contract DE-AC04-94AL85000. The authors appreciate the management support and guidance that we received in this effort. We thank

Dr. Vern Nicolette and Dr. Timothy O'Hern of SNL for reviewing this report. We also thank Prof. Chow of Hong Kong Polytechnic University for providing useful information regarding his pool fire experiment. The first author acknowledges that this research was conducted during his stay at SNL and wishes to acknowledge the partial support of this research by the New Faculty Research Grant, funded by the Korea University and Carbon Dioxide Reduction and Sequestration R & D Center (CDRS). The third author (Paul E. DesJardin) acknowledges the support of the National Science Foundation through grant CTS-0348110.

REFERENCES

1. G. Grant, J. Brenton, and D. Drysdale, Fire Suppression by Water Sprays, *Prog. Energy Combust. Sci.*, vol. 26, pp. 79–130, 2000.
2. D. J. Rasbash, Z. W. Rogowski, and G. W. V. Stark, Mechanisms of Extinction of Liquid Fires with Water Sprays, *Combust. Flame*, vol. 4, pp. 223–234, 1960.
3. A. A. Amsden, J. D. Ramshaw, P. J. O'Rourke, and J. K. Dukowicz, KIVA: A Computer Program for Two- and Three- Dimensional Fluid Flows with Chemical Reactions and Fuel Sprays, Los Alamos National Laboratory, Report No. LA-10245-MS, Los Alamos, NM, 1985.
4. P. E. DesJardin, T. J. O'Hern, and S. R. Tieszen, Large Eddy Simulation and Experimental Measurements of the Near-Field of a Large Turbulent Helium Plume, *Phys. Fluids*, vol. 16, pp. 1866–1883, 2004.
5. A. M. Lentati and H. K. Chelliah, Dynamics of Water Droplets in a Counterflow Field and Their Effect on Flame Extinction, *Combust. Flame*, vol. 115, 159–179, 1998.
6. C. C. Ndubizu, R. Ananth, P. A. Tatem, and V. Motevalli, On Water Mist Fire Suppression Mechanisms in a Gaseous Diffusion Flame, *Fire Safety J.*, vol. 31, pp. 253–276, 1998.
7. K. Prasad, C. Li, and K. Kailasanath, Optimizing Water-Mist Injection Characteristics for Suppression of Coflow Diffusion Flames, *27th Symposium (International) on Combustion*, The Combustion Institute, Pittsburgh, pp. 2847–2855, 1998.
8. K. Prasad, C. Li, K. Kailasanath, C. Ndubizu, R. Ananth, and P. A. Tatem, Numerical Modeling of Water Mist Suppression of Methane–Air Diffusion Flames, *Combust. Sci. Technol.*, vol. 132, pp. 325–364, 1998.

9. A. K. Lazzarini, R. H. Krauss, H. K. Chelliah, and G. T. Linteris, Extinction Conditions of Non-Premixed Flames with Fine Droplets of Water and Water/NaOH Solutions, *Proc. Combustion Inst.*, vol. 28, pp. 2939–2945, 2000.
10. H. K. Chelliah, A. K. Lazzarini, P. C. Wanigarathne, and G. T. Linteris, Inhibition of Premixed and Non-Premixed Flames with Fine Droplets of Water and Solutions, *Proc. Combustion Inst.*, vol. 29, pp. 369–376, 2002.
11. G. O. Thomas, The Quenching of Laminar Methane-Air Flames by Water Mists, *Combust. Flame*, vol. 30, pp. 147–160, 2002.
12. K. Prasad, C. Li, and K. Kailasanath, Simulation of Water Mist Suppression of Small Scale Methanol Liquid Pool Fires, *Fire Safety J.*, vol. 33, pp. 185–212, 1999.
13. C. T. Crowe, M. P. Sharma, and D. E. Stock, The Particle-Source-in-Cell (PSI-CELL) Model for Gas-Droplet Flows, *J. Fluids Eng.*, vol. 99, 325–332, 1977.
14. B. J. McCaffrey, Momentum Diffusion Flame Characteristics and the Effects of Water Spray, *Combust. Sci. Technol.*, vol. 63, pp. 315–335, 1989.
15. B. Downie and C. Polymeropoulos, Interaction of a Water Mist with a Buoyant Methane Diffusion Flame, *Fire Safety J.*, vol. 24, pp. 359–381, 1995.
16. G. Heskestad, Extinction of Gas and Liquid Pool Fires with Water Sprays, *Fire Safety J.*, vol. 38, pp. 301–317, 2003.
17. S. R. Tieszen, On the Fluid Mechanics of Fires, *Annu. Rev. Fluid Mech.*, vol. 33, pp. 67–92, 2001.
18. D. J. Rasbash and Z. W. Rogowski, Extinction of Fires in Liquids by Cooling with Water Mist, *Combust. Flame*, vol. 1, pp. 453–466, 1957.
19. L. Jianghong, L. Guangxuan, F. Weicheng, Y. Bin, and L. Xiyun, Study of Liquid Pool Fire Suppression with Water Mists by Cone Calorimeter, *J. Fire Sci.*, vol. 20, pp. 465–477, 2002.
20. R. L. Alpert, Calculated Interaction of Sprays with Large-Scale Buoyant Flows, *J. Heat Transfer*, vol. 106, pp. 310–317, 1984.
21. N. A. Hoffman and E. R. Galea, An Extension of the Fire-Field Modeling Technique to Include Fire-Sprinkler Interaction—I. The Mathematical Basis, *Int. J. Heat Mass Transfer*, vol. 36, pp. 1435–1444, 1993.

22. N. A. Hoffman and E. R. Galea, An Extension of the Fire-Field Modeling Technique to Include Fire-Sprinkler Interaction—II. The Simulations, *Int. J. Heat Mass Transfer*, vol. 36, pp. 1445–1457, 1993.
23. L. Y. Cooper and D. W. Stroup, Test results and predictions for the response of Near-Ceiling Sprinkler Links in a Full-Scale Compartment Fire, US Department of Commerce, National Bureau of Standards, NBSIR 87-3633, 1987.
24. W. K. Chow and N. K. Fong, Application of Field Modeling Technique to Simulate Interaction of Sprinkler and Fire-Induced Smoke Layer, *Combust. Sci. Tech*., vol. 89, pp. 101–151, 1993.
25. J. K. Dukowicz, A Particle-Fluid Numerical Model for Liquid Sprays, *J. Comput. Phys*., 35, 229–253, 1980.
26. C. Crowe, M. Sommerfeld, and Y. Tsuji, *Multiphase Flows with Droplets and Particles*, CRC Press, Boca Raton, 1998.
27. S. Nam, Numerical Simulation of the Penetration Capability of Sprinkler Sprays, *Fire Safety J*., vol. 32, pp. 307–329, 1999.
28. S. V. Patankar, *Numerical Heat Transfer and Fluid Flow*, Taylor & Francis, New York, 1980.
29. V. Novozhilov, D. J. E. Harvie, A. R. Green, and J. H. Kent, A Computational Fluid Dynamic Model of Fire Burning Rate and Extinction by Water Sprinkler, *Combust. Sci. Technol*., vol. 123, pp. 227–245, 1997.
30. P. E. DesJardin, L. A. Gritzo, and S. R. Tieszen, Modeling the Effect of Water Spray Suppression on Large Scale Pool Fires, *Halon Options Tech. Working Conf*., Albuquerque, May, 2000.
31. W. E. Ranz, and W. R. Marshall, Evaporation from Drops: Part I. *Chem. Eng. Prog*., vol. 48, pp. 141–146, 1952.
32. W. E. Ranz and W. R. Marshall, Evaporation from Drops: Part II. *Chem. Eng. Prog*., vol. 48, pp. 173–180, 1952.
33. A. H. Lefebvre, *Atomization and Sprays,* Hemisphere, New York, 1989.
34. K. M. Watson, Prediction of Critical Temperatures and Heats of Vaporization, *Ind. Eng. Chem*., vol. 23, pp. 360–364, 1931.
35. W. K. Chow and B. Yao, Numerical Modeling for Interaction of a Water Spray with Smoke Layer, *Numer. Heat Transfer, Part A*, vol. 39, pp. 267–283, 2001.

36. M. St-Georges and J. M. Buchlin, Detailed Single Spray Experimental Measurements and One-Dimensional Modeling, *Int. J. Multiphase Flow*, vol. 20, pp. 979–992, 1994.
37. J. Hua, K. Kumar, B. C. Khoo, and H. Xue, A Numerical Study of the Interaction of Water Spray with a Fire Plume, *Fire Safety J.*, vol. 37, pp. 631–657, 2002.
38. K. Prasad, G. Patnaik, and K. Kailasanath, A Numerical Study of Water–Mist Suppression of Large Scale Compartment Fires, *Fire Safety J.*, vol. 37, pp. 569–589, 2002.
39. J. A. Vaari, Transient One-Zone Computer Model for Total Flooding Water–Mist Fire Suppression in Ventilated Enclosures, *Fire Safety J.*, vol. 37, pp. 229–257, 2002.
40. J. L. Consalvi, B. Porterie, and J. C. Loraud, Dynamic and Radiative Aspects of Fire–Water Mist Interactions, *Combust. Sci. Tech.*, vol. 176, pp. 721–752, 2004.
41. V. Yakhot and S. Orszag Renormalization Group Analysis of Turbulence, *J. Sci. Comput.*, vol. 1, pp. 3–51, 1986.
42. S. C. Kim and H. S. Ryou, The Effect of Water Mist on Burning Rates of Pool Fire, *J. Fire Sci.*, vol. 22, pp. 305–323, 2004.
43. K. B. McGrattan, H. R. Baum, R. G. Rehm, A. Hamins, G. P. Forney, J. F. Floyd, and S. Hostikka, Fire Dynamics Simulator Version 3: Technical Reference Guide, NISTIR 6783, 2002.
44. Y. F. Li and W. K. Chow, Modelling of water mist fire suppression systems by a one-zone model, *Combust. Theory Model.*, vol. 8, pp. 567–592, 2004.
45. H. C. Kung, Cooling of Room Fires by Sprinkler Spray, *J. Heat Transfer*, vol. 99, pp. 353–359, 1977.
46. M. B. Kim, Y. J. Jang, and M. O. Yoon, Extinction Limit of a Pool Fire with a Water Mist, *Fire Safety J.*, vol. 28, pp. 295–306, 1997.
47. G. G. Back, C. L. Beyler, P. J. DiNenno, and R. Hansen, Full-Scale Water Mist Design Parameters Testing, US Cosat Guard, Report No. CG-D-03-99, Groton, CT, 1999.
48. C. C. Ndubizu, R. Ananth, and P. A. Tatem, The Effects of Droplet Size and Injection Orientation on Water Mist Suppression of Low and High Boiling Point Liquid Pool Fires, *Combust. Sci. Technol.*, vol. 157, pp. 63–86, 2000.

49. T. R. Marker and J. W. Reinhardt, *Water Spray as a Fire Suppression Agent for Aircraft Cargo Compartment Fires*, US Dept. of Transportation, Federal Aviation Administration (FAA), DOT/FAA/AR-TN01/1, Washington, DC, 2001.
50. W. K. Chow, Y. Gao, H. Dong, G. Zou, and L. Meng, Full-Scale Burning Tests on Heat Release Rate of Gasoline Fire with Water Mist, *J. Appl. Fire Sci.*, vol. 11, pp. 21–40, 2003.
51. W. P. Jones and B. E. Launder, 1972. The Prediction of Laminarization with a Two-Equation Model of Turbulence, *Int. J. Heat Mass Transfer*, vol. 15, pp. 301–314.
52. S. Ertesvag and B. F. Magnussen, The Eddy Dissipation Turbulence Energy Cascade Model, *Combust. Sci. Technol.*, vol. 159, pp. 213–235, 2000.
53. S. R. Tieszen and A. R. Black, Development of a Subgrid Fire Extinguishment Model, Technical Report No. SAND2001-3321, Sandia National Laboratories, Albuquerque, 2001.
54. J. C. Hewson, S. R. Tieszen, W. D. Sundberg, and P. E. DesJardin, CFD Modeling of Fire Suppression and Its Role in Optimizing Suppressant Distribution, *Proc. of 2003 Halon Options Tech. Working Conf.*, Albuquerque, HOTWC2003, New Mexico, 2003.
55. P. A. Tesner, Growth Rate of Soot Particles, *Combust. Sci. Technol.*, vol. 97, pp. 243–245, 1994.
56. P. E. DesJardin and L. A. Gritzo, A Dilute Spray Model for Fire Simulations: Formulation, Usage and Benchmark Problems, Sandia National Laboratories Technical Report No. SAND2002-3419, Albuquerque, 2002.
57. S. S. Yoon, J. C. Hewson, P. E. DesJardin, D. J. Glaze, A. R. Black, and R. R. Skaggs, Numerical Modeling and Experimental Measurements of a High Speed Solid-cone Water Spray for Use in Fire Suppression Applications, *Int. J. Multiphase Flow*, vol. 30, pp. 1369–1388, 2004.
58. M. R. Maxey and J. J. Riley, Equation of Motion for a Small Rigid Sphere in a Non-Uniform Flow, *Phys. Fluids*, vol. 26, pp. 883–889, 1983.
59. R. P. Chhabra, L. Agarwal, and N. K. Sinha, Drag on Non-Spherical Particles: An Evaluation of Available Methods, *Powder Technol.*, vol. 101, pp. 288–295, 1999.

60. G. H. Ganser, A Rational Approach to Drag Prediction of Spherical and Nonspherical Particles, *Powder Technol.*, vol. 77, pp. 143–152, 1993.
61. G. H. Ko, S. H. Lee, H. S. Ryou, and Y. K. Choi, Development and Assessment of a Hybrid Droplet Collision Model for Two Impinging Sprays, *Atomization and Sprays*, vol. 13, pp. 251–272, 2003.
62. T. L. Georjon and R. D. Reitz, A Drop-Shattering Collision Model for Multidimensional Spray Computations, *Atomization and Sprays*, vol. 9, pp. 231–254, 1999.
63. P. J. O'Rourke and A. A. Amsden, The TAB Method for Numerical Calculation of Spray Droplet Breakup, SAE Technical Paper No. 872089, 1987.
64. A. D. Gosman and E. Ioannides, Aspects of Computer Simulation of Liquid-Fueled Combustion, *19th AIAA Aerosp. Sci. Meeting*, St. Louis, MO, AIAA Paper No. AIAA-81-0323, 1981.
65. J. S. Shuen, L. D. Chen, and G. M. Faeth, Evaluation of a Stochastic Model of Particle Dispersion in a Turbulent Round Jet, *AIChE J.*, vol. 29, pp. 167–170, 1983.
66. A. Zhou and S. C. Yao, Group Modeling of Impacting Spray Dynamics, *Int. J. Heat Mass Transfer*, vol. 35, pp. 121–129, 1992.
67. G. M. Faeth, Mixing, Transport, and Combustion in Sprays, *Prog. Energy Combust. Sci.*, vol. 13, pp. 293–345, 1987.
68. J. Holen, B. Laksa, B. F. Magnussen, and B. E. Vembe, KAMELEON-II-Fire: A Description of the Mathematical Models, Numerical Methods and Solution Procedures, STF15-F94070, SINTEF Applied Thermodynamics, 1994.
69. R. J. Kee, F. M. Rupley, and J. D. Miller, CHEMKIN II: A Fortran Chemical Kinetics Package for the Analysis of Gas-Phase Chemical Kinetics, Technical Report SAND89-8009, Sandia National Laboratory, Livermore, CA, 1989.
70. P. Glaborg, R. J. Kee, J. F. Grcar, and J. Miller, PSR: A Fortran Program for Modeling Well Stirred Reactors, Technical Report No. SAND85-8209, Sandia National Laboratory, Livermore, CA, 1986.
71. S. R. Tieszen, D. W. Stamps, and T. J. O'Hern, A Heuristic Model of Turbulent Mixing Applied to Blowout of Turbulent Jet Diffusion Flames, *Combust. Flame*, vol. 106, pp. 442–466, 1996.

72. P. Koutmos, Simulations of Turbulent Methane Diffusion Flames with Local Extinction Effects, *Fluid Dyn. Res.*, vol. 24, pp. 103–119, 1999.
73. J. F.. Widmann, Characterization of a Residential Fire Sprinkler Using Phase Doppler Interferometry, *Atomization and Sprays*, 11, pp. 69–90, 2002.
74. S. R. Tieszen, T. J. O'Hern, E. J. Weckman, and R. W. Schefer, Experimental Study of the Effect of Fuel Mass Flux on a 1-m-diameter Methane Fire and Comparison with a Hydrogen Fire, *Combust. Flame*, vol. 139, pp. 126–141, 2004.
75. W. K. Chow, Atrium Smoke Exhaust and Technical Issues on Hot Smoke Tests, *ASME Summer Heat Transfer Conference*, July 17–22, San Francisco, ASME Paper No. HT2005-72412, 2005.